

# Competing automorphisms and disordered Floquet codes

Cory T. Aitchison<sup>1</sup> and Benjamin Béri<sup>1,2</sup>

<sup>1</sup>*DAMTP, University of Cambridge, Wilberforce Road, Cambridge, CB3 0WA, UK*

<sup>2</sup>*T.C.M. Group, Cavendish Laboratory, University of Cambridge, J.J. Thomson Avenue, Cambridge, CB3 0HE, UK*

Topological order is a promising basis for quantum error correction, a key milestone towards large-scale quantum computing. Floquet codes provide a dynamical scheme for this while also exhibiting Floquet-enriched topological order (FET) where anyons periodically undergo a measurement-induced automorphism that acts uniformly in space. We study disordered Floquet codes where automorphisms have a spatiotemporally heterogeneous distribution—the automorphisms “compete”. We characterize the effect of this competition, showing how key features of the purification dynamics of mixed codestates can be inferred from anyon and automorphism properties for any Abelian topological order. This perspective can explain the protection or measurement of logical information in a dynamic automorphism (DA) code when subjected to a noise model of missing measurements. We demonstrate this using a DA color code with perturbed measurement sequences. The framework of competing automorphisms captures essential features of Floquet codes and robustness to noise, and may elucidate key mechanisms involving topological order, automorphisms, and fault-tolerance.

## I. INTRODUCTION

Quantum error-correcting (QEC) codes are crucial for the effective, scalable operation of current and future quantum computers [1–9]. These codes envision a smaller number of protected logical qubits encoded within a larger Hilbert space of physical qubits. Similarly, quantum systems with long-range entanglement and topological order (TO) display robustness to local perturbations, host excitations with fractional statistics known as anyons, and support a topology-dependent ground-state degeneracy [10, 11]. Because of their inherent robustness, TOs are promising candidates for QEC codes.

These topological QEC codes have historically been static: the code properties, such as the stabilizer group in stabilizer codes [2, 12], are fixed through time. A recent class of codes, so-called dynamical codes, forgo this notion. They are inherently time-evolving and this can improve their characteristics or enable novel behaviors [13–16]. The first such example was the honeycomb code [17], a form of dynamical code called a Floquet code due to its time-periodic evolution. By measuring only two-qubit Pauli operators in a particular sequence, a stabilizer group emerges that enables the detection and correction of errors [18–20]. Each stage in the sequence generates a TO equivalent to a static toric code (TC) [21–24].

The close relationship between TOs and QEC has informed our understanding of both quantum matter and error-correction protocols. A prominent example is that of topological defects such as transparent domain walls, which permute the labels of anyon worldlines crossing the wall [25, 26]. These permutations, or “automorphisms”, are elements of the symmetry group of the anyons that preserves fusion and braiding data. In  $(2+1)\text{D}$  these domain walls terminate in point-like defects known as twists, which exhibit exotic behavior including anyon localization and enable topological quantum computation through their non-Abelian fusion and braiding [27, 28].

A key feature of the honeycomb Floquet code is that its measurement sequence implements a global automor-

phism every period that exchanges two of the  $TC$  anyons. The time-periodic nature of these automorphisms extend the TO to a time-crystalline-like phase [29]. This Floquet-enriched TO (FET) arises in dynamical codes through measurements, while FETs were originally proposed in unitarily driven  $(2+1)\text{D}$  TO systems [30, 31]. Dynamic automorphism (DA) codes extend this notion further by using measurement-induced automorphisms to construct quantum logic gates [32].

An important question is whether these FETs or codes are robust against perturbations or disorder. For the honeycomb code, recent results suggest competitive levels of tolerance to fabrication defects in realistic physical devices [33, 34], and that its FET persists amid random modifications to the measurement sequence, such as omitting or splitting up the two-qubit Pauli operators [35, 36]. Characterizing the effects of disorder in more general Floquet codes is, however, an open question. Previous results have largely focused on homogeneous cases concerning FETs with automorphisms acting globally [14, 26]. Analyses of topological defects in Floquet codes have primarily considered spatial domain walls [19, 20]. Perturbations to temporal domain walls—fundamentally modifying the Floquet evolution—were analyzed in terms of microscopic measurements in the honeycomb code [35, 36]. However, a framework capturing general aspects that follow from anyon data, i.e., a topological quantum field theory (TQFT) description of the dynamics, is missing.

Here we study Abelian TOs with measurement-induced automorphisms, and ask how do they evolve when perturbations cause the temporal domain walls to be spatiotemporally heterogeneous. These multiple domain walls, or “competing automorphisms”, nontrivially influence the codespace. We find that their evolution and purification dynamics are fundamentally decided by the homology classes of the domain walls’ boundary segments, and the properties of anyons that localize at the boundaries’ spatiotemporal twist defects or are invariant under the corresponding transition maps (that we

shall define in Section II). We show that such perturbed measurement-induced FETs can have rich phenomenology and form a new part of the landscape of quantum matter emerging from disordered measurements [36–54].

We also show how the framework of competing automorphisms can be used to characterize disordered dynamical QEC codes. To illustrate this, we explore how perturbations to the circuit protocol in the form of a noise model with missing measurements affects dynamic automorphism (DA) codes. Under this noise model, we show that the code’s ability to protect logical information can be readily understood via its competing automorphisms. We formulate necessary and sufficient conditions for different implementations of the DA color code to be unaffected by missing measurements, i.e., for a logical Hilbert subspace to remain unmeasured despite the disorder. Parameterizing the strength of the perturbations, we identify connections between the automorphisms of the code, and characterize the topological space of FETs in this exotic dynamical quantum matter. Our approach is generalizable to other dynamical codes and TOs understandable through their automorphisms.

The rest of the paper is organized as follows: in Section II, we provide background on FETs and the DA color code—we use this code as a motivating example and a concrete illustration for measurement-induced automorphisms. In Section III, we introduce competing automorphisms in dynamical quantum systems. In Section IV we then introduce a disordered DA color code and analyze its behavior using competing automorphisms. In Section V we conclude and discuss some future directions. Appendix A includes additional background material, while Appendix B discusses in more detail the disordered DA color code. Finally, Appendix C analytically and numerically examines the phases and critical behavior of the DA color code under our noise models.

## II. BACKGROUND

The color code topological order (CC) is defined on a 2D three-colorable lattice [25, 55–57]. In our work, we focus on the 6-6-6 honeycomb lattice formed by tessellating hexagonal plaquettes shown in Fig. 1. We color each plaquette red ( $r$ ), green ( $g$ ), or blue ( $b$ ) such that adjacent plaquettes are of different colors; a link that connects two plaquettes of the same color by convention adopts that color too. A qubit is placed on each lattice site and the Hamiltonian contains two species of commuting operators,  $P_X$  and  $P_Z$ , formed by the weight-6 Pauli  $X$  and Pauli  $Z$  tensor products on the corners of each hexagonal plaquette, with the identity elsewhere:

$$H_{CC} = - \sum_{\text{plaquette } p} P_{X,p} - \sum_{\text{plaquette } p} P_{Z,p}. \quad (1)$$

In the ground state of this Hamiltonian, a single-qubit Pauli operator at a lattice site excites three anyons in the

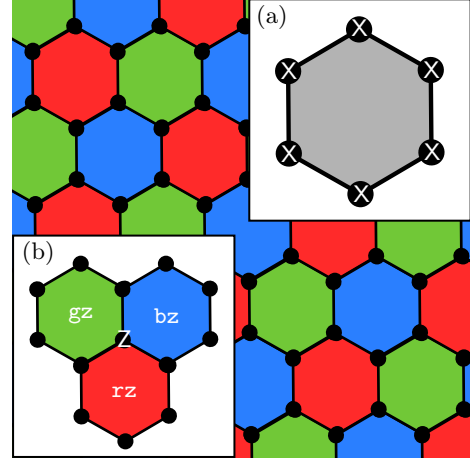


Figure 1. The 6-6-6 honeycomb lattice formed by hexagonal plaquettes, each assigned a color: red ( $r$ ), green ( $g$ ), or blue ( $b$ ). Links are colored by their terminating plaquettes; a link connecting two red plaquettes is also red, for example. A qubit (black circle) occupies each lattice site. Inset (a). The weight-6 operator  $P_X$  constructed from single-qubit Pauli  $X$  terms, used in the Hamiltonian. Inset (b). A single-qubit  $Z$  excites  $bz$ ,  $gz$ , and  $rz$  anyons in neighboring plaquettes.

three adjacent plaquettes, which we label by  $c\sigma$  indicating both the hosting plaquette color  $c \in \{r, g, b\}$  and the Pauli flavor  $\sigma \in \{x, y, z\}$  that created it. A single-qubit  $X$  therefore creates  $rx$ ,  $gx$ , and  $bx$  anyons, for example. An  $X$  applied to the two qubits of a red link creates a pair of  $rx$  anyons on the plaquettes at its endpoints.

These anyons and their behavior fundamentally define a TO. Self-statistics capture the topological or spin-statistics of a particle, while the mutual statistics encode the phase acquired upon braiding one anyon around another. In particular, bosons have trivial self-exchange statistics, fermions a  $-1$  statistic, while anyons can accumulate a different phase in  $U(1)$ . Mutual-semions accumulate a phase of  $-1$  when braided. The vacuum particle,  $1$ , is a boson and braids trivially with all other anyons. We have already encountered the 9 other, non-trivial, bosons of  $CC$ , formed by the combination of  $r, g, b$  colors and  $x, y, z$  flavors; two of these bosons that share the same color or flavor braid trivially, but otherwise are mutual-semions. There are also 6 fermions formed by pairs of mutual-semions; these are listed in Appendix A 1.  $CC$  is isomorphic to two copies of  $TC$ , written as  $CC \equiv TC \boxtimes TC$ , with  $\boxtimes$  denoting a product between two TOs; any anyon in  $CC$  can be written as a corresponding product of two anyons from  $TC$  [58–60].<sup>1</sup>

The anyon theory of a TO is also characterized by fusion rules (whereby two anyons in proximity to each other

<sup>1</sup> The toric code is characterized by four species of anyons: the vacuum  $1$ , bosons  $e$  and  $m$ , and fermion  $f$ . There are  $4^2$  anyon species in  $CC$  and  $4$  in  $TC$ .

are equivalent to a third) [61]. It is often convenient to represent the braiding and fusion rules of the color code by the “Mermin-Peres magic square” (hereafter referred to as the magic square) [62, 63]:

$$\begin{array}{c|cc|cc} rx & ry & rz \\ \hline gx & gy & gz \\ bx & by & bz \end{array} \quad (2)$$

such that bosons in the same row or column braid trivially while those that are not are mutual-semions. The fusion rules are such that two bosons in the same row or column fuse to make the third, and two anyons of the same type fuse (annihilate) to the vacuum. We write

$$rx \times rz = ry, \quad rz \times gz = bz, \quad gy \times gy = 1, \quad (3)$$

for example.

The automorphisms of a TO are maps between its anyon theories that preserve the statistics and fusion rules. For  $CC$ , these form a 72-element symmetry group  $\text{Aut}[CC]$  that is in correspondence to a subgroup of the permutations of the magic square:  $\text{Aut}[CC]$  can be decomposed<sup>2</sup> as  $(S_3 \times S_3) \rtimes S_2$  such that we can write any automorphism as the product of one of  $6 = 3!$  row or color permutations (the symmetry group  $S_3$ ), 6 column or flavor permutations ( $S_3$ ), and 2 color-flavor swapping reflections about the diagonal of the magic square ( $S_2$ ) [32]. Appendix A 2 provides a more detailed description of the relevant group-theoretic concepts of the automorphism group; we summarize some key information here. We denote elements of  $\text{Aut}[CC]$  using the cycle notation of the permutation group  $S_6$ , indicating the transformation of the 6 anyon labels  $r, g, b$ , and  $x, y, z$ . Since all bosons are composed of one color and one flavor label, cycles must always be formed of either disjoint color and flavor cycles, or alternating color and flavor.  $(rgx)(yz)$ , for example, is not a member of  $\text{Aut}[CC]$ , but  $(rx)(gy)(bz)$  and  $(rg)(xyz)$  are. We write the identity map as  $\text{id}$ . Composition of two elements of  $\text{Aut}[CC]$  are written as  $\varphi_2 \varphi_1$ , evaluated as  $(\varphi_2 \varphi_1)(a) = \varphi_2(\varphi_1(a))$  on some anyon  $a$ . The “separation” between two automorphisms  $\varphi_A, \varphi_B$  is quantified by the transition map

$$\tau_{BA} = \varphi_B \varphi_A^{-1}. \quad (4)$$

It links  $\varphi_B$  and  $\varphi_A$  by  $\varphi_B = \tau_{BA} \varphi_A$  and satisfies  $\tau_{AB} = \tau_{BA}^{-1}$ .  $\text{Aut}[CC]$  can be partitioned by cycle type into 9 conjugacy classes (sets that are linked by conjugation with some element in  $\text{Aut}[CC]$ ), which are subsets of the conjugacy classes of  $S_6$ . For example,  $(rg)(xyz)$  and  $(rgb)(xy)$  both contain one 2-cycle<sup>3</sup> and one 3-cycle and thus both have cycle type  $[2^1 3^1]$ . We denote their

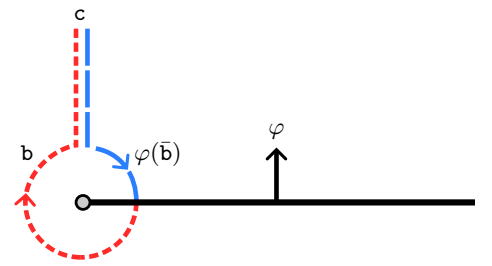


Figure 2. An anyon  $c$  decomposes into two anyons  $b$  and  $\varphi(\bar{b})$  in the vicinity of the endpoint (twist) of a domain wall. Moving anticlockwise around the endpoint enacts the automorphism  $\varphi$ . Since  $c$  can emanate or be absorbed at the twist, we say that  $c$  localizes at the  $\varphi$  twist. This picture applies to both temporal and spatial domain walls, and hence a time arrow is not indicated.

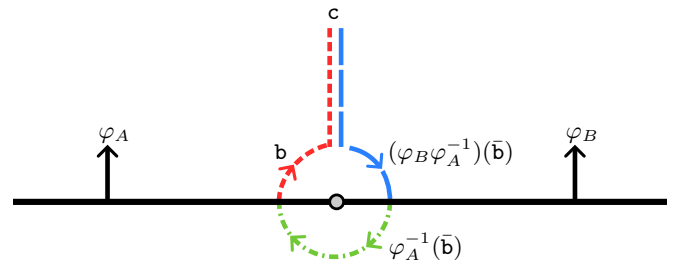


Figure 3. A  $\varphi_A$  and a  $\varphi_B$  domain wall separated by a boundary (indicated by the point). A  $c$  anyon that has fusion rule  $c = b \times (\varphi_B \varphi_A^{-1})(\bar{b})$  localizes at this boundary.

conjugacy class  $\mathcal{C}\{(ccc)(\sigma\sigma)\}$ . All 9 conjugacy classes are listed in Table I.  $\tau_{BA}$  and  $\tau_{AB}$  are in the same conjugacy class because permutations and their inverses are always of the same cycle type.

### A. Anyon Localization

A useful characterization for anyons is localization at domain wall endpoints (or “twists” [27]): if anyon  $c$  arises from fusion as  $c = b \times \varphi(\bar{b})$ , where  $\varphi$  is the domain wall automorphism for an anyon encircling a twist anticlockwise, it is said to localize at that twist by the process in Fig. 2 [25, 64]. At a  $\varphi_A$ - $\varphi_B$  boundary between two domain walls, anyon localization of  $c$  occurs if (cf. Fig. 3)

$$c = b \times \tau_{BA}(\bar{b}), \quad (5)$$

where  $\tau_{BA} = \varphi_B \varphi_A^{-1}$  is their transition map.

The number of anyons that can localize at a twist equals  $\mathcal{D}^2$ , the square of the quantum dimension  $\mathcal{D}$  of the twist.<sup>4</sup>  $\mathcal{D}$  tracks the increase in dimension of the

<sup>2</sup> The  $S_2$  subgroup is not closed under conjugation, and hence we require the semidirect product.

<sup>3</sup> A  $k$ -cycle is a cycle with  $k$  labels. It equivalently has order  $k$ : if  $\phi$  is a  $k$ -cycle then  $k \geq 1$  is minimal such that  $\phi^k = \text{id}$ .

<sup>4</sup> This relation applies only for Abelian anyon theories; in non-Abelian theories, one must also consider the quantum dimension of localizing anyons [25, 64, 65].

Table I. Conjugacy classes of the automorphism group,  $\text{Aut}[CC]$  (see Appendix A 2). Cycle type states the number of  $k$ -cycles that form the automorphisms, with  $[3^2]$  indicating two 3-cycles, for example.  $\mathcal{D}^2$  is the square of the quantum dimension of a twist, equal to the number of anyon species that localize at that twist (see Section II A). IMS indicates the number of invariant anyons that form mutual-semion pairs  $\mathbf{a}$  and  $\mathbf{b}$ , such that  $\varphi(\mathbf{a}) = \mathbf{a}$ ,  $\varphi(\mathbf{b}) = \mathbf{b}$ , with  $\mathbf{a}$  and  $\mathbf{b}$  having  $-1$ -mutual statistics, and trivial statistics with all other pairs.

Conjugacy Class	Cycle Type	Example	Parity on $S_3 \times S_3$	$\log_2 \mathcal{D}^2$	IMS	Number of Elements
$\mathcal{C}\{\text{id}\}$	$[1^6]$	$\text{id}$	even	0	4	1
$\mathcal{C}\{(\mathbf{c}\sigma)(\mathbf{c}\sigma)(\mathbf{c}\sigma)\}$	$[2^3]$	$(rx)(gy)(bz)$	even	1	2	6
$\mathcal{C}\{(\mathbf{ccc})(\mathbf{c}\sigma\sigma)\}$	$[3^2]$	$(rgb)(xyz)$	even	2	2	4
$\mathcal{C}\{(\mathbf{cc})(\mathbf{c}\sigma\sigma)\}$	$[1^2 2^2]$	$(rg)(xy)$	even	2	0	9
$\mathcal{C}\{(\mathbf{c}\sigma\sigma\mathbf{c}\sigma)\}$	$[6^1]$	$(rxgybz)$	even	3	0	12
$\mathcal{C}\{(\mathbf{ccc})\}$	$[1^3 3^1]$	$(rgb)$	even	4	0	4
$\mathcal{C}\{(\mathbf{cc})\}$	$[1^4 2^1]$	$(rg)$	odd	2	0	6
$\mathcal{C}\{(\mathbf{c}\sigma\sigma)(\mathbf{c}\sigma)\}$	$[2^1 4^2]$	$(rxgy)(bz)$	odd	3	0	18
$\mathcal{C}\{(\mathbf{ccc})(\mathbf{c}\sigma\sigma)\}$	$[1^1 2^1 3^1]$	$(rgb)(xy)$	odd	4	0	12
Total						72

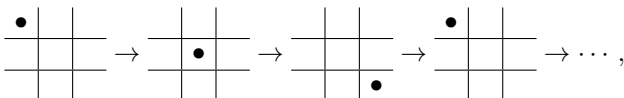
Hilbert space when twists are introduced. If  $\mathbf{c}$  localizes at  $\tau_{BA}$ , then for any automorphism  $\varphi$ ,  $\varphi(\mathbf{c})$  localizes at  $\varphi\tau_{BA}\varphi^{-1}$ . Hence, the quantum dimension of an automorphism's twist is a characteristic of its conjugacy class. Table I lists  $\log_2 \mathcal{D}^2$  for each conjugacy class in  $\text{Aut}[CC]$ .

In Section III, we examine how twists at the boundaries of temporal domain walls affect the TO. In comparison to existing works such as Refs. 14, 20, 25, and 26, which considered homogeneous or spatial domain walls, we focus on heterogeneous temporal domain walls. We show that anyon localization in this context fundamentally leads to logical measurements of the degenerate codespace when the FET is operated as a QEC code.

## B. Anyon Condensation

Anyon condensation is the process of relating two topologically-ordered systems by identifying a set of condensed bosons in the “parent” TO with the vacuum particle in the “child” TO [26, 66–71]; the process has similarities to its namesake Bose-condensations in other physical systems [67].

Condensing a nontrivial boson,  $\mathbf{c}\sigma$ , in a  $CC$  parent phase realizes a child theory equivalent to the toric code TO, denoted as  $TC(\mathbf{c}\sigma)$  [26]. By condensing different bosons at different times, a system transitions between different child theories. Indeed, the honeycomb Floquet code is equivalent to a dynamical transition through the TOs of  $TC(\mathbf{rx}) \rightarrow TC(\mathbf{gy}) \rightarrow TC(\mathbf{bz}) \rightarrow TC(\mathbf{rx}) \rightarrow \dots$  [17]. We diagrammatically represent this sequence using the magic square notation of Eq. (2),



such that the  $\bullet$  indicates the condensed boson.

Importantly, two child theories  $TC(\mathbf{c}\sigma_1)$  and  $TC(\mathbf{c}\sigma_2)$  are compatible if and only if  $\mathbf{c}\sigma_1$  and  $\mathbf{c}\sigma_2$  are mutual-

semions [32, 72, 73]. This ensures that two regions of  $TC(\mathbf{c}\sigma_1)$  and  $TC(\mathbf{c}\sigma_2)$  in spacetime share an invertible domain wall: if we start with  $TC(\mathbf{c}\sigma_1)$  and condense the  $\mathbf{c}\sigma_2$  boson, the quantum state of the TO is preserved. Any anyon in  $TC(\mathbf{c}\sigma_1)$  can move across the domain wall and be mapped onto another anyon in  $TC(\mathbf{c}\sigma_2)$  without modifying information about the particle (such as its statistics with other anyons). This process of pairing up consecutive compatible child theories  $TC(\mathbf{c}\sigma_1) \rightarrow TC(\mathbf{c}\sigma_2)$  is called a “reversible transition”. In the magic square notation, reversible transitions require that consecutive stages condense bosons that share neither the same row nor the same column.

It is also possible to construct a TO where anyon condensation results in a child  $CC$  theory. One such example is the “dynamic automorphism” (DA) color code from Ref. 32, using a parent  $CC \boxtimes CC$  theory of two color code models; this can be envisaged as the honeycomb lattice with two qubits at each lattice site (or equivalently, two layers of honeycomb lattices) each hosting an independent  $CC$  phase. The Hamiltonian is equivalent to Eq. (1), except there are now two of each  $P_X$  and  $P_Z$  that act only on the first or second layers. Condensing the anyons  $\mathbf{rz}_1\mathbf{rz}_2$ ,  $\mathbf{gy}_1\mathbf{gy}_2$ , and thus  $\mathbf{bz}_1\mathbf{bz}_2$  (where the subscripts indicate the layer) produces a child theory  $\widetilde{CC}$  equivalent to the color code.<sup>5</sup> The anyons of this theory have representatives

$$\begin{array}{|c|c|c|} \hline \mathbf{rx}_1\mathbf{rx}_2 & \mathbf{ry}_1\mathbf{rx}_2 & \mathbf{rz}_1 \\ \hline \mathbf{gx}_1\mathbf{gx}_2 & \mathbf{gy}_1\mathbf{gx}_2 & \mathbf{gz}_1 \\ \hline \mathbf{bx}_1\mathbf{bx}_2 & \mathbf{by}_1\mathbf{bx}_2 & \mathbf{bz}_1 \\ \hline \end{array} \sim \begin{array}{|c|c|c|} \hline \mathbf{ry}_1\mathbf{ry}_2 & \mathbf{rx}_1\mathbf{ry}_2 & \mathbf{rz}_2 \\ \hline \mathbf{gy}_1\mathbf{gy}_2 & \mathbf{gx}_1\mathbf{gy}_2 & \mathbf{gz}_2 \\ \hline \mathbf{by}_1\mathbf{by}_2 & \mathbf{bx}_1\mathbf{by}_2 & \mathbf{bz}_2 \\ \hline \end{array} \quad (6)$$

in correspondence to the  $CC$  anyons of Eq. (2), with  $\sim$  indicating equivalence up to fusion with the condensed bosons. For example,  $\mathbf{rx}_1\mathbf{rx}_2 \times \mathbf{rz}_1\mathbf{rz}_2 = \mathbf{ry}_1\mathbf{ry}_2$ . When

<sup>5</sup> This is only one such condensation choice; we could condense  $x$ -flavored bosons, for example, and achieve an equivalent theory.

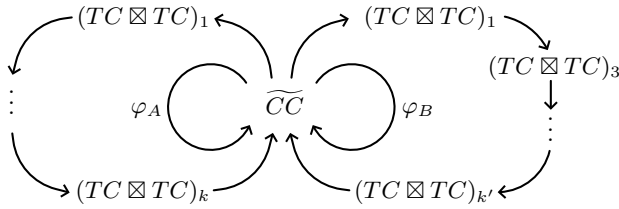


Figure 4. A color code topological order ( $\widetilde{CC}$ ) can be mapped through a series of doubled toric code topological orders ( $TC \boxtimes TC$ ) via anyon condensation. Upon returning to the original  $\widetilde{CC}$ , an automorphism  $\varphi_A$  permutes the anyons of the model, creating a Floquet-enriched topological order (FET). Modifying the sequence, such as by skipping  $(TC \boxtimes TC)_2$ , may result in a different automorphism,  $\varphi_B$ .

referring to anyons of  $\widetilde{CC}$ , if the subscripts are omitted then we are denoting them by their equivalent sectors in  $CC$ ; that is,  $\mathbf{rx}$  refers to  $\mathbf{rx}_1\mathbf{rx}_2$  or  $\mathbf{ry}_1\mathbf{ry}_2$ .

Condensing an individual anyon from each  $CC$  layer alternatively creates a child theory of two decoupled toric codes, denoted  $TC(\mathbf{c}\sigma_1) \boxtimes TC(\mathbf{c}\sigma_2)$  with  $\boxtimes$  again indicating the tensor product. Reversible transitions now occur in two ways: (1)  $TC \boxtimes TC \leftrightarrow TC \boxtimes TC$  are reversible iff the individual  $TC_1$  and  $TC_2$  transitions are reversible; and (2)  $\widetilde{CC} \leftrightarrow TC \boxtimes TC$  are reversible iff the two condensed anyons of the  $TC \boxtimes TC$  are of different colors and neither are  $z$ -flavored<sup>6</sup> [32].

Automorphisms can be implemented by transitioning through a series of condensations, cf. Fig. 4. Davydova et al. [32] showed how sequences starting and ending at  $\widetilde{CC}$  can transition the TO in such a way that any of the 72  $\text{Aut}[CC]$  automorphisms can be enacted using at most 4 intermediary  $TC \boxtimes TC$  condensations. For example, this is a sequence that enacts an  $(rgb)$  automorphism,

$$\widetilde{CC} \rightarrow \begin{array}{|c|c|} \hline 1 & \\ \hline 2 & \\ \hline \end{array} \rightarrow \begin{array}{|c|c|} \hline & 2 \\ \hline 1 & \\ \hline \end{array} \rightarrow \begin{array}{|c|c|} \hline 2 & \\ \hline 1 & \\ \hline \end{array} \rightarrow \widetilde{CC} \quad (7)$$

where the 1, 2 labels indicate the condensed boson in the two  $CC$  layers, using the magic square notation from Eq. (2). That is, this sequence of anyon condensation maps between the TOs of  $\widetilde{CC} \rightarrow TC(\mathbf{rx}_1) \boxtimes TC(\mathbf{bx}_2) \rightarrow TC(\mathbf{bx}_1) \boxtimes TC(\mathbf{gz}_2) \rightarrow TC(\mathbf{gy}_1) \boxtimes TC(\mathbf{ry}_2) \rightarrow \widetilde{CC}$ . Appendix A 4 explains how to compute the automorphism from any given sequence, or construct a sequence to realize any given automorphism. By repeatedly cycling through a sequence of condensates such as Eq. (7) similarly to a driven quantum system, we thus create

an evolving phase that exhibits time-periodic, Floquet-enriched topological order (FET) [30]. Anyons present will periodically have their labels permuted. Multiple measurement sequences can realize the same automorphism each Floquet period, and therefore multiple different systems can exhibit the same FET.

### C. Dynamical Codes

We may also interpret these FETs as dynamical QEC codes capable of encoding and storing quantum information. The first dynamical code was the honeycomb Floquet code from Ref. 17. Other dynamical codes have since been proposed, such as the CSS honeycomb code [14, 26], the automorphism code [29], the dynamic automorphism color code [32], the  $x+y$  Floquet code [74], the XYZ ruby code [75],  $(3+1)D$  Floquet codes [76], or the hyperbolic Floquet code [77]. Theoretical studies of dynamical codes include perspectives such as subsystem codes [14, 65], quantum cellular automata [72], twist-defect networks [78], adiabatic paths of Hamiltonians [29], or fixed-point path integrals [79–82], and aspects of Floquet code phenomenology were also linked to symmetry topological field theory [83].

To describe such codes, we use here the stabilizer formalism [2, 7, 12, 84]: taking the  $P_X$  and  $P_Z$  plaquette Hamiltonian terms from Eq. (1), we promote them to generators of an Abelian “stabilizer” group  $\mathcal{S}$ .<sup>7</sup> The simultaneous  $+1$ -eigenspace of  $\mathcal{S}$  defines the codespace  $C$  such that  $\forall S \in \mathcal{S}$  and  $|\psi\rangle \in C$  we have  $S|\psi\rangle = |\psi\rangle$ .  $C$  coincides with the ground space of our Hamiltonian. Excited states  $|\psi'\rangle$ , for which  $S|\psi'\rangle = -|\psi'\rangle$  for some  $S \in \mathcal{S}$ , are not in the codespace; the “excited” stabilizers indicate that the system has suffered an error. These excited plaquettes are equivalent to the locations of anyon excitations in the Hamiltonian picture. Logical operators map between states within the degenerate codespace  $C$ ; these are denoted as  $\bar{X}, \bar{Z}$  and act with the same algebra on the (logical) Hilbert space of  $C$  as  $X, Z$  act on single qubits. The centralizer of  $\mathcal{S}$  is the group  $C(\mathcal{S})$  of Pauli operators that commute with every stabilizer; the nontrivial logicals are those in  $C(\mathcal{S})$  but not in (a phase times)  $\mathcal{S}$  itself, forming the set  $\mathcal{L} = C(\mathcal{S}) \setminus \langle i\mathbb{1}, \mathcal{S} \rangle$ .

To perform anyon condensation, we use projective measurements of the hopping operators for the condensed boson; these are (typically) weight-2 Pauli operators that correspond to moving an excitation through the lattice [26]. For a  $\mathbf{rx}$  in the color code, for example, it is the 2-qubit  $X$  operator on the ends of a red link. Measuring these throughout a system in the codespace of  $CC$  causes a  $CC \rightarrow TC(\mathbf{rx})$  transition [26]. In doing so, the

<sup>6</sup> This condition arises due to the choice of  $z$ -flavored condensations leading to the child theory  $\widetilde{CC}$ .

<sup>7</sup> A stabilizer group is specifically any subgroup of the  $n$ -qubit Pauli group that does not contain  $-1$  and where all the elements commute. It “stabilizes” a code in the sense that any element of the stabilizer group acts trivially on the logical subspace.

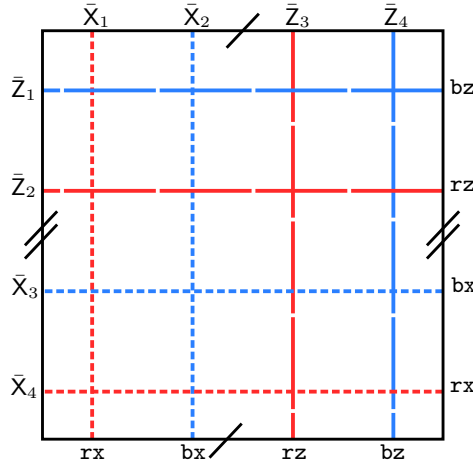


Figure 5. Diagram of the logical operators of the  $CC$  model on a 2-torus. Shown are the 4 pairs of anticommuting  $X$  (short-dashed) and  $Z$  (long-dashed) operators from Eq. (8)-(11), supported on noncontractible cycles of the 2-torus. The honeycomb lattice structure is ignored for simplicity; the string operators follow the red and blue links of Fig. 1.

stabilizer group updates as measured operators are added and anticommuting operators are combined or removed; since this group is constantly changing in a dynamical code, we refer to the current state as the instantaneous stabilizer group (ISG) [17]. The ISG updates during each condensation stage.

In our work, we focus on the  $CC \boxtimes CC$  model of the DA color code. In this context, the external tensor product denotes that the stabilizer group of  $CC \boxtimes CC$  can be factored (up to a unitary transformation) into two independent copies of  $CC$  stabilizer groups [32]. The initial stabilizer group is thus comprised of  $P_X$  and  $P_Z$  plaquettes on both layers of honeycomb lattices. Forming the child theory  $\widetilde{CC}$  requires projective measurements of  $Z_1 Z_2$  on each lattice site, where the subscripts indicate the two layers.  $TC \boxtimes TC$  child theories are analogous to the previous discussions, with hopping operators measured on each layer separately for the respective condensed anyons.

Our implementation of the DA color code uses a 2-torus; future work may find it fruitful to consider other topologies or open boundary conditions. We employ a logical algebra with 4 pairs of anticommuting logical operators constructed out of  $rx$ ,  $bz$ ,  $bx$ , and  $rz$  effective anyon strings. Two operators are equivalent (act equivalently on the codestates) if they are related modulo multiplication with operators in the stabilizer group [2]. This means that multiple representatives of each logical operator exist; on the 2-torus these are supported on homologous noncontractible cycles around the periodic boundaries.<sup>8</sup> Let  $\bar{O}[a]_h$  and  $\bar{O}[a]_v$  represent the equivalence

class of logical operators, forming the quotient group  $C(\mathcal{S})/\mathcal{S}$ . The subscript indicates that the string wraps around the horizontal or vertical direction respectively (using the orientation of Fig. 1). An italicized  $\bar{O}[a]_h$  indicates a particular representative of the equivalence class. We use the logical algebra

$$\bar{X}_1 = \bar{O}[rx]_v, \quad \bar{Z}_1 = \bar{O}[bz]_h, \quad (8)$$

$$\bar{X}_2 = \bar{O}[bx]_v, \quad \bar{Z}_2 = \bar{O}[rz]_h, \quad (9)$$

$$\bar{X}_3 = \bar{O}[bx]_h, \quad \bar{Z}_3 = \bar{O}[rz]_v, \quad (10)$$

$$\bar{X}_4 = \bar{O}[rx]_h, \quad \bar{Z}_4 = \bar{O}[bz]_v. \quad (11)$$

Figure 5 shows sketches of these operators. An automorphism that permutes the anyons now also permutes the logical operators. ( $rb$ ), for example, swaps  $\bar{X}_1$  and  $\bar{X}_2$ , and is indeed equivalent to a  $\text{SWAP}_{12}\text{SWAP}_{34}$  gate on the four qubits. The 72 automorphisms furnish a subgroup of the 4-qubit Clifford group [32]. This choice of logical algebra is not unique. Indeed, we are also not restricted to just using bosons; any choice of 4 anyons that form two pairs of mutual-semions but otherwise have trivial mutual statistics (hence commuting string operators) can form a valid logical algebra. Section IV B, for example, describes an alternative logical algebra using fermions.

### III. COMPETING AUTOMORPHISMS

In this section, we introduce systems of disordered Floquet codes where the temporal domain walls are spatially heterogeneous: acting on disjoint subregions of the manifold with different automorphisms. As the realization of such subregions is random, we can interpret this as two (or more) automorphisms “competing” for occupancy of the system. We first describe the effect of one realization of this competition on Abelian-anyon TOs, before extending our results to measurement-induced FETs where different realizations of the automorphisms occur at every discrete timestep. We use  $CC$  as an example TO, in preparation for Section IV where we examine a disordered DA color code from this perspective.

Consider a 2-torus (although our results are readily generalizable to other topologies with different genera) and assume at time  $t = 0$  the system is in the ground-state of some local Hamiltonian  $H = -\sum_j S_j$  with local generators  $S_j$  of a stabilizer group  $\mathcal{S}$ . The manifold is randomly partitioned, and each contiguous region labeled  $A$  or  $B$ . At time  $0 < t_\varphi < 1$ , automorphisms  $\varphi_A$  and  $\varphi_B$  ( $\varphi_A \neq \varphi_B$ , and one of which may be trivial) are simultaneously applied to their respective subregions. We may equivalently view this as  $\varphi_A$  applied everywhere and  $B$ -subregions additionally enacting  $\tau_{BA}$ .

Global automorphisms implemented via homogeneous temporal domain walls map ground states of  $H$  to ground

<sup>8</sup> Two cycles are homologous if one can be smoothly deformed into

the other without breaking the chain. A cycle is noncontractible if it is not homologous to a loop with zero area, i.e. a point.

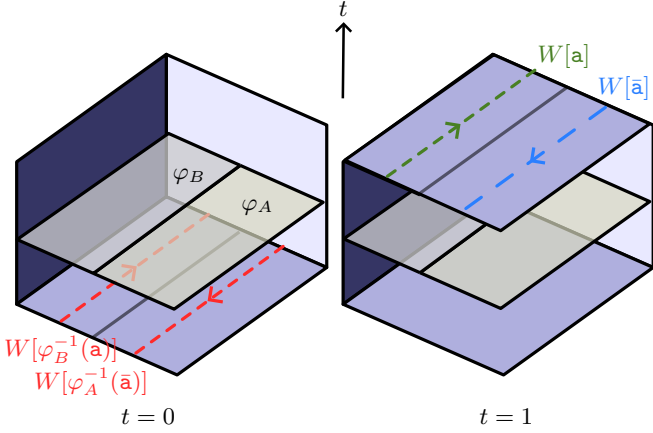


Figure 6. Spacetime illustration of a section of an Abelian TO, with time flowing upwards, where  $\varphi_A$  and  $\varphi_B$  domain walls act concurrently on disjoint regions of the lattice between times  $t = 0$  and  $t = 1$ . The operator  $O_0 = W[\varphi_B^{-1}(\mathbf{a})]W[\varphi_A^{-1}(\bar{\mathbf{a}})]$  with support straddling a (closed) segment of the  $\varphi_A$ - $\varphi_B$  boundary evolves to the product  $O_1 = W[\mathbf{a}]W[\bar{\mathbf{a}}]$  at  $t = 1$ . This is a stabilizer.

states. This is not true of heterogeneous domain walls, however, as the automorphism boundaries may bisect the local stabilizer terms. In this case, the resulting system may no longer be a ground state (or eigenstate) of  $H$ . If the system is then projected back into an eigenstate of  $H$ , this may result in a nontrivial (potentially non-unitary) mapping. This projection is precisely that expected when performing QEC on a stabilizer code, as error-detection measurements ensure that a system returns to stabilizer eigenstates.<sup>9</sup>

The key consequence of the competing automorphisms is that logical operators and stabilizers interchange, which in QEC codes can lead to measurement of encoded information. To see this, consider a closed segment of the boundary between  $\varphi_A$  and  $\varphi_B$  domain walls. Let  $W[\mathbf{a}]$  denote a Wilson loop operator for some anyon  $\mathbf{a}$  along this segment. Take the operator

$$O_0 = W[\varphi_B^{-1}(\mathbf{a})]W[\varphi_A^{-1}(\bar{\mathbf{a}})], \quad (12)$$

cf. Fig. 6. If the  $A$ - $B$  boundary is noncontractible and

$$\varphi_B^{-1}(\mathbf{a}) \times \varphi_A^{-1}(\bar{\mathbf{a}}) \neq 1, \quad (13)$$

or equivalently

$$\mathbf{d} \equiv \mathbf{a} \times \tau_{BA}(\bar{\mathbf{a}}) \neq 1, \quad (14)$$

then  $O_0$  is a logical operator. At  $t = t_\varphi$ , this operator will evolve to

$$O_1 = W[\mathbf{a}]W[\bar{\mathbf{a}}], \quad (15)$$

<sup>9</sup> In this analysis, for ease of presentation, we imagine automorphisms and stabilizer measurements occurring at different times. In dynamical code implementations, such as the DA color code, these two processes typically occur concurrently.

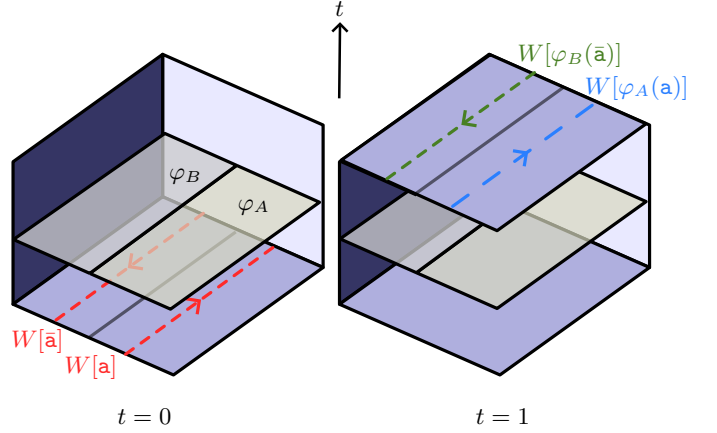


Figure 7. At  $t = 0$ , operator  $Q_0 = W[\mathbf{a}]W[\bar{\mathbf{a}}]$  with support straddling  $\mathbf{a}$  (closed) segment of the  $\varphi_A$ - $\varphi_B$  boundary is in the stabilizer group. By  $t = 1$ , this operator evolves to the (potentially nontrivial)  $Q_1 = W[\varphi_A(\mathbf{a})]W[\varphi_B(\bar{\mathbf{a}})]$ .

which is a stabilizer in  $\mathcal{S}$  as  $\mathbf{a} \times \bar{\mathbf{a}} = 1$ . This means that if the system was in a superposition of eigenstates of the logical operator  $O_0$ , it is now by  $t = 1$  in the same superposition of eigenstates of  $O_1$ , a stabilizer. Moreover, if this were a QEC code, this  $O_1$  will be measured during syndrome detection, and eventually be corrected into a  $+1$ -eigenstate by QEC. Information encoded by the logical operator  $O_0$  will thus be measured out.

At the same time, consider the stabilizer

$$Q_0 = W[\mathbf{a}]W[\bar{\mathbf{a}}], \quad (16)$$

cf. Fig. 7. This evolves into

$$Q_1 = W[\varphi_A(\mathbf{a})]W[\varphi_B(\bar{\mathbf{a}})] \quad (17)$$

at  $t = 1$ . If the boundary is again noncontractible and

$$\varphi_A(\mathbf{a}) \times \varphi_B(\bar{\mathbf{a}}) \neq 1, \quad (18)$$

or equivalently,

$$\mathbf{c} \equiv \mathbf{b} \times \tau_{BA}(\bar{\mathbf{b}}) \neq 1, \text{ where } \mathbf{b} \equiv \varphi_A(\mathbf{a}), \quad (19)$$

then  $Q_1$  is a logical operator. Since  $Q_0$  was a stabilizer, this  $Q_1$  logical operator will have a  $+1$ -eigenvalue at  $t = 1$ , regardless of the encoded state at  $t = 0$ .

Together, these processes show that logical operators and stabilizers interchange (sketched in Fig. 8). Since the sizes of the stabilizer group and logical operators remain constant between  $t = 0$  and  $t = 1$  (as automorphisms are unitary operations) then we must have that for every logical operator that maps onto a stabilizer, a stabilizer must map onto a logical operator.<sup>10</sup> Moreover,

<sup>10</sup> There is a related behavior whereby local stabilizers (that is, their

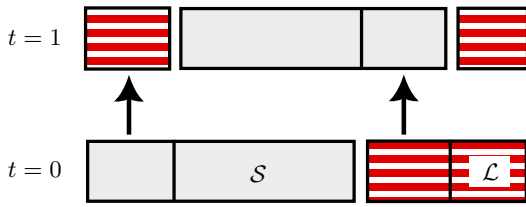


Figure 8. Schematic of the stabilizer group  $\mathcal{S}$  (grey boxes) and logical operators  $\mathcal{L}$  (red striped boxes) before ( $t = 0$ ) and after ( $t = 1$ ) a round of competing automorphisms. If the domain wall boundaries contain noncontractible segments, then some stabilizers map onto logical operators and vice versa. Each independent (up to fusion) nontrivial anyon that localizes at  $\tau_{BA}$  twists leads to another logical operator that gets exchanged with a stabilizer. These logical operators adopt the  $+1$ -eigenvalues of the stabilizers that map onto them. During syndrome measurement, these exchanged logical operators will also be measured.

from Eq. (5),  $\mathbf{c}$  and  $\mathbf{d}$  are precisely anyons that localize at the  $\tau_{BA} = \varphi_B \varphi_A^{-1}$  twists. Hence, for every independent (under fusion) nontrivial anyon  $\mathbf{c}$  that localizes, if the  $\varphi_A$ - $\varphi_B$  boundary contains noncontractible segments, a logical operator and stabilizer interchange, leading to the measurement of encoded information.

For a  $\mathbb{Z}_2$  TO, such as  $TC$  or  $CC$ , with each anyon its own antiparticle, and for a  $\tau_{BA}$  with quantum dimension  $\mathcal{D}$ ,  $\log_2 \mathcal{D}^2$  indicates the number of independent nontrivial anyon strings introduced to the ISG at a  $\varphi_A$ - $\varphi_B$  boundary segment; when at least one such segment is noncontractible,  $\log_2 \mathcal{D}^2$  is also the number of logical qubits measured. As noted in Sec. II A, this number is a property of the  $\tau_{BA}$  conjugacy class. For example,  $\mathcal{C}\{(c\sigma)(c\sigma)(c\sigma)\}$  is the only conjugacy class for  $\text{Aut}[CC]$  that measures exactly one logical qubit,  $\log_2 \mathcal{D}^2 = 1$ ; the one nontrivial localized anyon for an automorphism  $(c_1\sigma_1)(c_2\sigma_2)(c_3\sigma_3)$  is the fermion  $c_1\sigma_1 \times c_2\sigma_2 \times c_3\sigma_3$ .

How are the other logical operators affected by the competing automorphisms? Intuitively, one may imagine that an anyon that transforms identically under both automorphisms,  $\varphi_A(\mathbf{a}) = \varphi_B(\mathbf{a})$ , would be unaffected by the domain wall boundary. In such a case, the logical would simply transform as

$$\bar{O}[\mathbf{a}] \mapsto \bar{O}[\varphi_A(\mathbf{a})], \quad (20)$$

regardless of the domain wall configurations. The existence of such a logical is equivalent to there existing

an anyon  $\mathbf{b} = \varphi_A(\mathbf{a})$  such that  $\mathbf{b} = \tau_{BA}(\mathbf{b})$ , i.e.,  $\mathbf{b}$  is invariant under  $\tau_{BA}$ . We can extend this idea to show the existence of logical operators that are unaffected by competing automorphisms, using the lemma (proven in Appendix A 3):

**Lemma 1.** *For an automorphism  $\tau$  and anyon  $\mathbf{b}$ ,  $\mathbf{b} = \tau(\mathbf{b})$  if and only if  $\mathbf{b}$  and  $\mathbf{c}$  braid trivially for all anyons  $\mathbf{c}$  that localize at  $\tau$ .*

Any anyon  $\mathbf{d}$  that is not invariant under  $\tau_{BA}$  must braid nontrivially with a localized anyon, and therefore logical operator  $\bar{O}[\mathbf{d}]$  will be measured out if the competing automorphisms have a noncontractible boundary segment dual to the cycle following the support of  $\bar{O}[\mathbf{d}]$ . Conversely, if  $\mathbf{b}_1$  and  $\mathbf{b}_2$  are mutual-semions that are both invariant under  $\tau_{BA}$ , then neither  $\mathbf{b}_1$  nor  $\mathbf{b}_2$  can localize at  $\tau_{BA}$ . The logical operators  $\bar{O}[\mathbf{a}_1]_v$  and  $\bar{O}[\mathbf{a}_2]_h$  [with  $\mathbf{b}_1 = \varphi_A(\mathbf{a}_1)$ ,  $\mathbf{b}_2 = \varphi_A(\mathbf{a}_2)$ ] anticommute, forming a logical  $\bar{X}$  and  $\bar{Z}$  that satisfy Eq. (20). Moreover, they do not map onto one of the measured  $W[\mathbf{c}]$   $\varphi_A$ - $\varphi_B$  boundary-operators, and they also commute with all such measurements. The existence of a mutual-semion pair invariant under  $\tau_{BA}$  thus guarantees a logical qubit that is not measured or overwritten in any realization of competing  $\varphi_A$  and  $\varphi_B$  domain walls. We call this a “protected” logical qubit.<sup>11</sup> Since both  $(\bar{O}[\mathbf{a}_1]_v, \bar{O}[\mathbf{a}_2]_h)$  and  $(\bar{O}[\mathbf{a}_1]_h, \bar{O}[\mathbf{a}_2]_v)$  form anticommuting  $\bar{X}$  and  $\bar{Z}$  pairs, on a 2-torus we in fact have two protected qubits per invariant mutual-semion pair. If an anyon  $\mathbf{b}$  is invariant under  $\tau_{BA}$ , then for any automorphism  $\varphi$ ,  $\varphi(\mathbf{b})$  is invariant under the conjugate automorphism  $\varphi\tau_{BA}\varphi^{-1}$ . Hence, the number of independent invariant mutual-semion pairs and protected qubits also characterizes the conjugacy class of  $\tau_{BA}$ . For  $\tau_{BA} \in \text{Aut}[CC]$ , the only conjugacy classes with such pairs are  $\mathcal{C}\{\text{id}\}$ ,  $\mathcal{C}\{(c\sigma)(c\sigma)(c\sigma)\}$  and  $\mathcal{C}\{(ccc)(\sigma\sigma\sigma)\}$ , cf. Table I. For example,  $\tau_{BA} = (rx)(gy)(bz)$  has  $\mathbf{rx}$  and  $\mathbf{bz}$  as invariant mutual-semions.

Localized and invariant anyons thus characterize the extent to which logical information is lost over one period of competing automorphisms. The number of independent nontrivial localized anyons,  $\log_2 \mathcal{D}^2$ , indicates the number of logical qubits measured if the boundaries of the competing automorphisms contain noncontractible segments. Boundary segments along homologous non-contractible cycles support representatives of the same measured logical operator. The number of invariant mutual-semions (IMS) is the number of logical qubits that are protected and will not be measured out, regardless of the particular domain wall configurations. For example, if  $\log_2 \mathcal{D}^2 = 2$  and  $\text{IMS} = 0$  for the  $CC$  model on the 2-torus, then for a given domain wall configuration

supports are confined to a ball of constant radius relative to the linear system size), such as plaquettes, that straddle the  $A$ - $B$  boundary map onto operators that create pairs of  $\mathbf{c}$  excitations. When these stabilizers are measured, they will be re-added to the stabilizer group along with a random  $\pm 1$  phase. The product of these phases around a noncontractible  $A$ - $B$  boundary segment is precisely the phase of the measured logical operator.

<sup>11</sup> If invariant anyons do not form a mutual-semion pair, then information may not be protected. For example, if  $\tau_{BA} = (rg)$  in  $CC$ , then its invariant anyons  $\mathbf{bx}$ ,  $\mathbf{by}$ , and  $\mathbf{bz}$  all braid trivially. Moreover, they all localize, e.g.,  $\mathbf{bx} = \mathbf{rx} \times (rg)(\mathbf{gx})$ , and are thus measured out along noncontractible boundary segments.

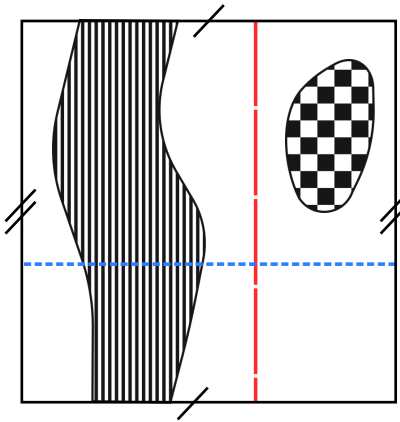


Figure 9. A 2-torus showing two temporal domain walls. If the boundary of a domain wall has only contractible segments (checked region), there exists at least one representative of each logical operator (red and blue lines) that avoids intersecting the boundary. On the other hand, a domain wall with a noncontractible boundary segment (striped region) always bisects one of each  $\bar{X}$ ,  $\bar{Z}$  logical operator pairs.

2 of the 4 qubits will not be measured out between  $t = 0$  and  $t = 1$ . However, the same 2 qubits may be measured in a different configuration, since  $W[c]$  along each of the 2 noncontractible cycles span the logical space.<sup>12</sup> On the other hand, if  $\text{IMS} = 2$  then that means that the same 2 logical qubits are protected in any disorder realization.<sup>13</sup>

What about multiple consecutive realizations of competing automorphisms? Consider that between  $t = 1$  and  $t = 2$  we again (randomly) partition the manifold and enact  $\varphi_A$  and  $\varphi_B$ . Assume that the  $\varphi_A$ - $\varphi_B$  boundaries contain noncontractible segments such that logical operators are measured. If a protected logical qubit exists from  $t = 0$  to  $t = 2$ , there must be mutual-semions that braid trivially with the anyons  $c$  that localize at  $\tau_{BA}$  between  $t = 0$  and  $t = 1$ . They must also braid trivially with the anyons that will localize between  $t = 1$  and  $t = 2$ , that is  $\varphi_A^{-1}(c)$  or  $\varphi_B^{-1}(c)$ . If all localized anyons braid trivially,<sup>14</sup> then Lemma 1 tells us that  $\varphi_A^{-1}(c) = \varphi_B^{-1}(c)$ . Extending this argument to  $t \rightarrow \infty$ , we therefore have two protected logical qubits for each pair of mutual-semions that braid trivially with  $\varphi_A^{-t}(c)$  for  $t = 0, 1, 2, \dots$  and for all  $c$  that localize at  $\tau_{BA}$ . If not all localized anyons have trivial mutual statistics,<sup>15</sup> then requiring that the mutual-semions braid trivially with all  $(\varphi_t \varphi_{t-1} \cdots \varphi_1)(c)$  where

<sup>12</sup> This occurs when localized anyons braid trivially with each other.

<sup>13</sup> The conclusions in this paragraph use the fact that domain wall boundaries cannot contain two disjoint cycles that simultaneously encircle orthogonal noncontractible cycles of the 2-torus. Otherwise, it would be possible to measure out all 4 logical qubits when  $\log_2 \mathcal{D}^2 = 2$  in just one domain wall instance.

<sup>14</sup> In CC, this is guaranteed whenever there is a single nontrivial localized anyon,  $\log_2 \mathcal{D}^2 = 1$ .

<sup>15</sup> In CC, nontrivial mutual statistics is required for  $\log_2 \mathcal{D}^2 > 1$ .

each  $\varphi_i \in \{\varphi_A^{-1}, \varphi_B^{-1}\}$  and  $t = 0, 1, 2, \dots$  is a sufficient condition for a protected logical qubit.

These behaviors discussed are dependent only on the presence of noncontractible boundary segments in the domain walls, not on the specific microscopic details. This allows us to characterize systems of competing automorphism by their homology. We label a realization of  $\varphi_A$  and  $\varphi_B$  temporal domain walls as  $\varphi_A$ -dominant if the  $A$ -labelled subregions can completely contain a noncontractible cycle from every homology class. That is, the support of a representative of each logical operator can be contained within the  $A$ -subregions.  $\varphi_B$ -dominant configurations are defined analogously. In these cases, Eq. (20)—with  $\varphi = \varphi_A$  or  $\varphi_B$  respectively—holds for a representative of each logical operator. Moreover, the  $\varphi_A$ - $\varphi_B$  boundaries must have only contractible segments, hence logical information is not necessarily lost or measured.<sup>16</sup> However, if the  $\varphi_A$ - $\varphi_B$  boundaries contain noncontractible segments, such as in Fig. 9,<sup>17</sup> then at least one logical operator is measured corresponding to the nontrivial anyons that localize at  $\tau_{BA}$ .

Competing automorphisms lead to the measurement of logical information, and can therefore be naturally applied to explain the purification dynamics of disordered Floquet codes. Specifically, we envision a Floquet code initialized into a completely mixed logical state. Subjected to repeated rounds of heterogeneous temporal domain walls, the average number of logical qubits measured or protected each timestep can be inferred directly by the conjugacy classes of the automorphism transition maps and the homology classes of the cycles contained within the domain wall subregions. This can equivalently be applied to a fixed initial logical state, and the question of how long logical information can remain protected despite the heterogeneous dynamics. In the following section, we use this information to discuss the behavior of a disordered dynamical code. In Appendix C we explore in more detail the purification dynamics of these codes using numerical simulations.

#### IV. DISORDERED DA COLOR CODES

Section III showed that heterogeneity in the temporal domain walls of Floquet codes can lead to the purifi-

with  $\text{IMS} > 0$ , otherwise four commuting logicals can be measured on conjugate noncontractible  $\varphi_A$ - $\varphi_B$  boundary cycles.

<sup>16</sup> Such a domain wall contains a representative of each of the torus' noncontractible cycles. Cutting open the torus along one of each cycle turns the manifold into a square with open boundaries, which now contains the (uncut) boundary segments of the domain wall. These segments must thus all be contractible.

<sup>17</sup> In addition to the example striped region in Fig. 9, the boundary might alternatively contain a noncontractible segment extending around both cycles of the torus. In this case, the measured logical operator is equivalent to a product of  $\bar{O}_v$  and  $\bar{O}_h$  logical operators using the algebra in Fig. 5. The resulting behavior is therefore analogous to the case discussed here.

cation of mixed codestates or, equivalently, the loss of logical information. In this section, we show that this picture can readily be applied to a class of noise models that affect the evolution of dynamic automorphism (DA) codes, helping characterize their resilience to disorder.

In addition to common noise models such as depolarizing channels or circuit-level noise [5, 8, 22, 85–87], to characterize the fault-tolerance of a QEC code and the stability of its underlying TO one should also consider the effect of perturbations to the circuit protocol. In measurement-induced FETs such as DA codes, this can occur via missing measurements. Ref. 35, for example, considered the effect of missing parity measurements in the honeycomb Floquet code, finding that the FET phase persisted up to a critical point despite the disorder. Beyond this, noise models incorporating missing measurements have been poorly understood in the literature, despite being a relevant failure mode for quantum devices.

Unlike circuit-level noise, missing measurements can theoretically be tracked with perfect knowledge by a classical operator of a quantum computer: a measurement that does not occur may produce no classical output bit. With perfect knowledge, is it not then trivial to correct for errors that arise from missing measurements? If the circuit protocol is able to adaptively and immediately repeat any measurements without output bits this may be easily overcome. Such on-the-fly adaptivity, however, may introduce classical bottlenecks and be impractical to implement in systems involving extensive measurements such as Floquet codes. Repeated measurements are not able to be parallelized, for example, and allow other errors (such as Pauli errors) to accumulate while waiting for imperfect measurements to succeed. It would be beneficial if the effect of missing measurements could be “swept under the rug” by the topological protection of the code, in the same way that Pauli errors are able to be corrected if their weight is below a threshold [22]. This may also allow us to optimize the circuit protocol, if, for example, we can purposefully skip measurements on some nonvanishing subset of the physical qubits while still enacting the desired automorphism gate.

What about correcting the errors after each round of error-detection, incorporating missing-measurement correction alongside syndrome correction? This is reminiscent of the problem in  $[[n, k, d]]$  stabilizer codes when the locations of random Pauli errors are known (called “located” errors in Ref. 86). In this case, weight  $d - 1$  errors can be corrected, instead of just  $\lfloor \frac{d-1}{2} \rfloor$ . Since in topological codes  $d$  is the length of the manifold’s shortest nontrivial cycle, this is a geometric condition, similar to whether competing automorphisms have noncontractible boundary segments. Missing measurements, as we will argue, can result in competing automorphisms, and correspond to similar geometric considerations regarding their capacity to remove logical information.

In the honeycomb Floquet code, erasure channels [88]—with depolarizing noise occurring at known locations—below a certain error rate can be effectively

corrected [89]. Similarly, with missing measurements in Floquet codes the protection of logical information should persist up to a critical point (Ref. 35 showed this for the honeycomb Floquet code). There also exists protected logical subspaces that are unaffected by missing measurements, even beyond this critical point. As we will show, this stems directly from Floquet codes with missing-measurement noise models being systems with competing automorphisms.

For a nontrivial illustration, we focus now on the behavior of the DA color codes [32] when perturbed by stochastic missing measurements. This picture can analogously be interpreted as instead randomly including additional measurements. Recall that in Section II we introduced DA color codes as a sequence of condensed anyons that correspond to link measurements on a two-layered honeycomb lattice. To add disorder to a given stage of measurements, for each associated link on the lattice we independently include that link in the measurement sequence with probability  $p \in [0, 1]$ . Otherwise, it is omitted. If we assume that the initial sequence consists of only reversible pairs of condensations—that is, it is a valid implementation of the DA color code—then it is not guaranteed that removing one measurement sequence retains this reversibility. Consider Eq. (7), for example. Focusing on the  $\mathbf{bz}_1$  condensations in the third stage, we denote the disordered sequence in the shorthand

$$\begin{array}{c} \widetilde{CC} \\ \rightarrow \end{array} \begin{array}{c} | \\ 1 \\ \hline | \\ 2 \\ \hline \end{array} \rightarrow \begin{array}{c} | \\ 2 \\ \hline | \\ 1 \\ \hline \end{array} \rightarrow \begin{array}{c} | \\ 2 \\ \hline | \\ 1 \\ \hline \end{array} \underbrace{\rightarrow}_{p} \begin{array}{c} | \\ 2 \\ \hline | \\ 1 \\ \hline \end{array} \rightarrow \widetilde{CC}. \quad (21)$$

When  $p = 0$ , no  $\mathbf{bz}_1$  links are measured and we follow the sequence

$$\widetilde{CC} \rightarrow \begin{array}{c} | \\ 1 \\ \hline | \\ 2 \\ \hline \end{array} \rightarrow \begin{array}{c} | \\ 2 \\ \hline | \\ 1 \\ \hline \end{array} \rightarrow \begin{array}{c} | \\ 2 \\ \hline | \\ 1 \\ \hline \end{array} \rightarrow \widetilde{CC},$$

which enacts a valid  $(rxgybz)$  automorphism (see Appendix A 4 for an explanation of deriving this automorphism). When  $p = 1$  we measure all the  $\mathbf{bz}_1$  links and follow

$$\widetilde{CC} \rightarrow \begin{array}{c} | \\ 1 \\ \hline | \\ 2 \\ \hline \end{array} \rightarrow \begin{array}{c} | \\ 2 \\ \hline | \\ 1 \\ \hline \end{array} \rightarrow \begin{array}{c} | \\ 2 \\ \hline | \\ 1 \\ \hline \end{array} \rightarrow \widetilde{CC},$$

with automorphism  $(rgb)$ . In this way, the presence of measured  $\mathbf{bz}_1$ -links across the lattice defines disjoint regions of  $(rxgybz)$  and  $(rgb)$  temporal domain walls, completely analogous to the discussion of competing automorphisms in Section III. Figure 10 depicts this relationship using a spacetime illustration.

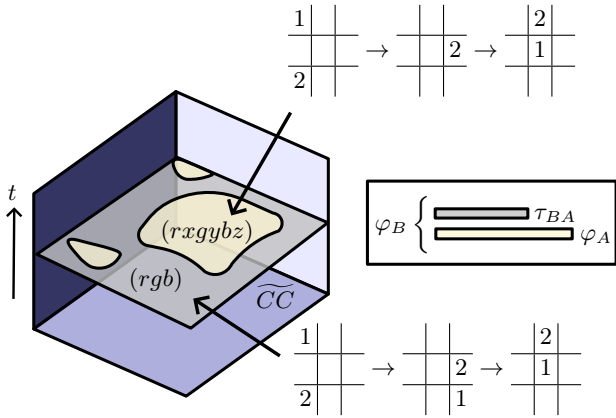


Figure 10. Spacetime illustration of one period of the 1-component disorder model from Eq. (21), with two competing automorphisms:  $\varphi_A = (rxgybz)$  and  $\varphi_B = (rgb)$ . Time runs upwards and the spatial planes represent timeslices of the  $\widehat{CC}$  TO. The  $(rgb)$  domain wall is the dominant region, containing the support of noncontractible cycles, characteristic of the supercritical disordered phase. The inset shows the perspective where we enact a  $\varphi_A$  domain wall everywhere, and only the transition map  $\tau_{BA}$  forms clusters.

On the other hand, if we modify the sequence to

$$\begin{aligned}
 \widehat{CC} &\rightarrow \begin{array}{|c|c|} \hline 1 & \\ \hline 2 & \\ \hline \end{array} \rightarrow \begin{array}{|c|c|} \hline & 2 \\ \hline & 1 \\ \hline \end{array} \rightarrow \begin{array}{|c|c|} \hline & 1 \\ \hline & 2 \\ \hline \end{array} \\
 &\rightarrow \begin{array}{|c|c|} \hline 2 \\ \hline \textcolor{red}{1} \\ \hline \end{array} \rightarrow \widehat{CC}, \tag{22}
 \end{aligned}$$

then when  $p = 0$  there is an irreversible condensation  $rx_1 \rightarrow gx_1$ . This sequence therefore does not produce a transparent domain wall or enact an automorphism. In general, there are two possible irreversible scenarios: “intralayer”  $TC_i \rightarrow TC_i$  irreversible condensations ( $i = 1, 2$ ); and “interlayer”  $TC \boxtimes TC \leftrightarrow \widehat{CC}$  irreversible condensations. Such irreversibility means that anyons of the effective child theory are condensed, creating punctures in the TO [26]. If the affected regions cannot enclose noncontractible cycles, then, with knowledge of where missing measurements occurred,<sup>18</sup> in theory these patches can be reinitialized later thus restoring the original code without affecting the logical information. Otherwise, logical information will be lost. The effects of such irreversible condensations on the code are discussed

further in Appendix B 3. For the remainder of this section, we focus on measurement sequences that are inherently immune to this behavior: missing any measurement stage will—by construction—not introduce any irreversible condensations. This avoids the potential for irreparable damage to the codespace, focusing on the errors that are correctable. One question that we address by the end of this section is precisely what this limitation leaves us in terms of potential automorphisms that can still be constructed in this way. If that set is large enough, this limitation may be beneficial in informing the design of DA color code quantum circuits that are robust against missing measurements.

Limiting our systems to just those that produce differing automorphisms at different realizations of the disorder, we can interpret them as models of competing automorphisms from Section III. Understanding what automorphisms can arise in the different outcomes of disorder can therefore inform us as to which logical operators are measured or protected, if any. Let  $\varphi_A$  be the automorphism enacted when  $p = 0$ , and  $\varphi_B$  when  $p = 1$ . When the  $\varphi_A$ - $\varphi_B$  boundaries contain a noncontractible path, we expect that logical information is measured. Microscopically, the measured logical operators here are formed from the links at the boundary of the disordered stage and the immediately-preceding condensate in the same  $CC$  layer. In Eq. (21), for example, the measured anyon after the disordered  $bz_1$  condensations is the fermion  $rx_1 \times bz_1$ . Following the condensations forward to  $\widehat{CC}$  at  $t = 1$ , this fermion updates to become  $rx_1 ry_2 \times bz_1$ , which is equivalent to the  $ry \times bz$  fermion in  $\widehat{CC}$ . This is precisely the anyon that localizes at  $\tau_{BA} = (rgb) \cdot (rxgybz)^{-1} = (rz)(gx)(by)$ . The corresponding logical operators are the  $O[ry \times bz]$  vertical or horizontal operators in the  $\widehat{CC}$  phase at  $t = 1$  (or  $O[by \times gz]$  at  $t = 0$ ). Because the string is formed from the product of links set by the disorder, there is exactly one anyon species measured.

We also saw in Section III that protected logical operators correspond to the invariant mutual-semion pairs of  $\tau_{BA}$ . In our example, Table I shows one such pair for  $\tau_{BA}$ , and therefore there exists a 2-qubit logical Hilbert subspace that remains unaffected by the missing measurements. We note that in an analysis of the simpler honeycomb Floquet code, Ref. 35 also found that fermionic string operators were measured around the boundaries of missing-measurement regions. Their discussion relied on specific microscopic details of the measurement sequence, however, whereas our perspective of competing automorphisms is detail-agnostic and generalizable to other Abelian-anyon FETs, while also allowing us to intuit further details such as the presence of protected logical qubits.

Since the size of each domain wall subregion is directly determined by the value of the parameter  $p$ , we can associate certain regions in phase-space with the different behaviors of the  $\varphi_A$ - $\varphi_B$  boundaries. For some critical value  $p_c \in [0, 1]$ , we have:

<sup>18</sup> If we are alerted to a missing measurement, we can determine if an irreversible condensation occurred by referencing the measurement schedule and checking if the preceding and following condensed bosons (that are not missed) braid trivially.

- (1) **Subcritical phase:**  $p < p_c$  such that with high probability the configuration is  $\varphi_A$ -dominant.
- (2) **Critical point:**  $p \sim p_c$  such that with high probability a  $\varphi_A$ - $\varphi_B$  boundary contains noncontractible segments.
- (3) **Supercritical phase:**  $p > p_c$  such that with high probability the configuration is  $\varphi_B$ -dominant.

In the thermodynamic limit of  $L \rightarrow \infty$ , one—and only one—logical qubit is measured out only at the critical point  $p = p_c$  of this disorder model. Whether only one logical degree of freedom is measured out over multiple periods depends on the structure of subsequent disorder partitions as well as the properties of the automorphisms; these cases are discussed in Section IV B. The value of  $p_c$  and the critical behavior of the model are discussed further in Appendix C. We find that the systems show transitions in the universality class of bond percolation on kagome or triangular lattices; this is consistent with earlier works examining missing measurements in the simpler honeycomb Floquet code [35].

### A. Connected FETs

To understand the effect of missing measurements on the DA color code, we first simplify our noise model further by assuming that only one stage of the measurement sequence is disordered. We call this a “1-component disorder model” with a parameter  $p$ ; all the examples given thus far fall in this category. In Section IV C we generalize our results to the case where multiple—or all—stages may contain missing measurements. We are concerned with two important behaviors: (1) what automorphisms can be realized while maintaining only reversible condensation sequences; and (2) what the requirements are for there to exist protected logical subspaces, despite the disorder. We focus on the first question in this section, and address the second in Section IV B.

To answer this, we introduce the following definitions:

**Definition 1** (Adjacent FETs). *Two FETs  $A$  and  $B$  with automorphisms  $\varphi_A$  and  $\varphi_B$  are adjacent if there exists a 1-component disorder model that realizes competing  $\varphi_A$  and  $\varphi_B$  temporal domain walls.*

**Definition 2** (Connected FETs). *Two FETs,  $A_0$  and  $A_m$ , are connected if there exists an adjacency sequence of FETs  $\{A_0, A_1, \dots, A_m\}$ , such that  $A_i$  and  $A_{i+1}$  are adjacent for all  $i = 0, \dots, m-1$ . The length of this sequence is defined as  $m$ .*

It is worth clarifying here that we are working in a space of FETs in which they are labeled solely by their automorphisms. Hence, distinct measurement sequences realizing the same automorphism are identified. If two FETs are adjacent, it does not guarantee that there is a 1-component disorder model involving any given two

measurement sequences realizing FETs  $A$  and  $B$ . Rather, at least one exists. Similarly, with connected FETs, for each  $j = 1, \dots, m-1$ , we allow for FET  $A_j$  to be realized by distinct measurement sequences in the 1-component disorder models connecting it to  $A_{j-1}$  and to  $A_{j+1}$ .<sup>19</sup>

We argued previously that at criticality a 1-component disorder model measures exactly one logical qubit (with high probability). By Section III, this necessitates that  $\tau_{BA}$  has  $\log_2 \mathcal{D}^2 = 1$ . From Table I, for  $\text{Aut}[CC]$  there is only one conjugacy class for which this is true. Two FETs in the DA color code are thus adjacent only if their automorphisms satisfy the *separation condition*

$$\tau_{BA} \in \mathcal{C}\{(c\sigma)(c\sigma)(c\sigma)\}. \quad (23)$$

There are several immediate consequences of this:

- (1) The trivial FET,  $\mathbb{1}$ , with  $\varphi = \text{id}$  is adjacent only to FETs with automorphisms in the  $\mathcal{C}\{(c\sigma)(c\sigma)(c\sigma)\}$  conjugacy class. This follows from  $\varphi_B = \tau_{BA} \cdot \text{id}$ .
- (2) Adjacent FETs always have different parities on the  $S_2$  subgroup of  $\text{Aut}[CC]$  (color-flavor exchange, c.f. Appendix A 2b), but the same parities on the  $S_3 \times S_3$  subgroup (color or flavor permutations). This comes from  $\tau_{BA}$  having odd-parity on the  $S_2$  subgroup, but even-parity on the  $S_3 \times S_3$  subgroup.
- (3) Two FETs in the same conjugacy class are never adjacent, since elements of a conjugacy class have the same parities on all subgroups.
- (4) The logical operator that is measured when the system is tuned near the critical point must be a fermion string. This is because there is precisely one nontrivial anyon—a fermion—that localizes at twists corresponding to the automorphisms in  $\mathcal{C}\{(c\sigma)(c\sigma)(c\sigma)\}$  [25]. For a  $(c_1\sigma_1)(c_2\sigma_2)(c_3\sigma_3)$  automorphism, this fermion is  $c_1\sigma_1 \times c_2\sigma_2 \times c_3\sigma_3$ .

We can promote this separation condition to a sufficient and necessary condition by showing that for all FET pairs with automorphisms satisfying Eq. (23) there exists a measurement sequence and 1-component disorder model that connects them. We first introduce the idea of concatenating two measurement sequences: let  $\mathcal{A}_i, \mathcal{C}_j$  denote some  $TC \boxtimes TC$  child theories. For a sequence

$$\widetilde{CC} \rightarrow \mathcal{A}_1 \rightarrow \dots \rightarrow \mathcal{A}_m \rightarrow \widetilde{CC} \quad (24)$$

that realizes automorphism  $\varphi_A$ , and a sequence

$$\widetilde{CC} \rightarrow \mathcal{A}_m \rightarrow \mathcal{C}_1 \rightarrow \dots \rightarrow \mathcal{C}_n \rightarrow \widetilde{CC} \quad (25)$$

---

<sup>19</sup> In a space that distinguishes distinct measurement sequences, different measurement sequences realizing the same FET may not be connected in the sense of Definition 2, see App. B 2.

that realizes automorphism  $\varphi_C$ , we can construct the concatenated sequence

$$\widetilde{CC} \rightarrow \mathcal{A}_1 \rightarrow \cdots \rightarrow \mathcal{A}_m \rightarrow C_1 \rightarrow \cdots \rightarrow C_n \rightarrow \widetilde{CC} \quad (26)$$

that realizes automorphism  $\varphi_C \varphi_A$ . Now, the trivial FET,  $\mathbb{1}$ , is adjacent to all FETs in  $\mathcal{C}\{(c\sigma)(c\sigma)(c\sigma)\}$ ; we explicitly provide example 1-component disorder models in Appendix B 1 to prove this. Then, let  $A$  and  $B$  be any two FETs with automorphisms  $\varphi_A$  and  $\varphi_B$  that satisfy the separation condition,  $\tau_{BA} \in \mathcal{C}\{(c\sigma)(c\sigma)(c\sigma)\}$ . It is possible (see Appendix A 4) to construct a measurement sequence for  $A$  such that its final  $TC \boxtimes TC$  child theory is the same as the first  $TC \boxtimes TC$  child theory of the measurement sequence that connects  $\text{id}$  and  $\tau_{BA}$  via a 1-component disorder model. Using the result above, we concatenate the measurement sequence for  $A$  with the measurement sequence that realizes  $\varphi_C = \text{id}$  or  $\varphi_C = \tau_{BA}$ . We now have a 1-component disorder model that creates automorphisms  $\varphi_A = \text{id} \cdot \varphi_A$  and  $\varphi_B = \tau_{BA} \varphi_A$ . Thus, two FETs are adjacent if and only if their automorphisms satisfy Eq. (23).

We now build towards an understanding of what automorphisms can be realized while maintaining just 1-component disorder models: for example, are any two arbitrary FETs connected? Equivalently, constructing the graph  $G = (N, E)$  with each node in  $N$  a distinct FET and an edge in  $E$  joining adjacent FETs, is this graph connected? If two nodes  $n, m \in N$  are joined by an edge, then their automorphisms  $\varphi_n, \varphi_m$  satisfy  $\tau_{mn} \in \mathcal{C}\{(c\sigma)(c\sigma)(c\sigma)\}$ . By Section IV A,  $\varphi_m = \tau_{mn} \varphi_n$  has the same parity on  $S_3 \times S_3$  as  $\varphi_n$ . There is thus no path in  $G$  connecting two FETs with automorphisms of different parity on  $S_3 \times S_3$ , and  $G$  has (at least) two non-empty connected components. Each component contains 36 FETs, grouped by the conjugacy class of their automorphisms (cf. Table I).<sup>20</sup>

We numerically compute all inequivalent 1-component disorder models by enumerating the possible isomorphism contributions (see Appendix A 4), thus specifying the graph  $G$ . Figure 11 shows the minimum graph distances on  $G$  between all FETs, as well as displaying the separation into exactly two connected components.

We can explain these graph distances, starting from the simple case of transitions from the trivial FET: We begin with the sequence of two adjacent FETs  $\{\mathbb{1}, A_1\}$ . Using a 1-component disorder model, if  $A_1$  is adjacent to the trivial FET then its automorphism  $\varphi_1$  satisfies  $\varphi_1 = \tau_{10} \cdot \text{id} = \tau_{10}$ , where  $\tau_{10} \in \mathcal{C}\{(c\sigma)(c\sigma)(c\sigma)\}$ . Any automorphism in  $\mathcal{C}\{(c\sigma)(c\sigma)(c\sigma)\}$  can be realized from

<sup>20</sup> There is no direct interpretation of these two components in terms of logical gates. In particular, the mapping from automorphisms to gates is intrinsically dependent on the geometry and boundary conditions of the manifold. For a fixed algebra on the 2-torus, each automorphism can be written as a logical gate in the 4-qubit Clifford group. No apparent structure emerges, however, when viewing these gates grouped by their parity.

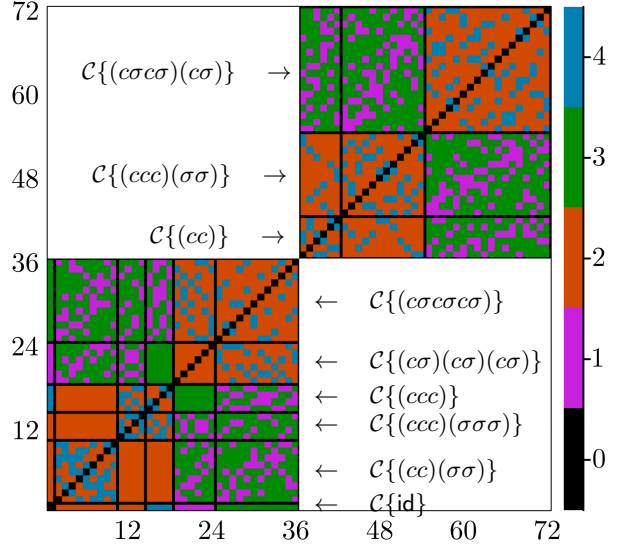


Figure 11. Each row and column corresponds to one of the 72 automorphisms in  $\text{Aut}[CC]$ , grouped by conjugacy class. The color indicates the minimum number of edges connecting the nodes in  $G$  associated with the row and column automorphisms; equivalently, it is the length of the minimum adjacency sequence connecting the two FETs of those automorphisms. There are two distinct clusters, grouped by their parity on the  $S_3 \times S_3$  subgroup; even-parity automorphisms are in the bottom left quadrant and odd-parity in the top right quadrant. White squares indicate that there is no possible adjacency sequence to connect those two FETs.

the identity using a 1-component disorder model. Since these automorphisms exchange color and flavor, we can interpret  $\tau_{10}$  geometrically as a reflection of the magic square (placed on a 2-torus) along a mirror line parallel to the diagonal or antidiagonal. Specifically, the mirror line intersects the three bosons listed by the three 2-cycles of the automorphism.  $(ry)(gz)(bx)$ , for example, has a mirror line through anyons  $\text{ry}$ ,  $\text{gz}$ , and  $\text{bx}$ .

For a sequence  $\{\mathbb{1}, A_1, A_2\}$ , the associated automorphism for  $A_2$  must satisfy  $\varphi_2 = \tau_{21} \varphi_1 = \tau_{21} \tau_{10}$ , where both  $\tau_{21}, \tau_{10} \in \mathcal{C}\{(c\sigma)(c\sigma)(c\sigma)\}$  are such reflections. If  $\tau_{21} = \tau_{10}$  we arrive back at  $\text{id}$ . Otherwise, there are two scenarios to consider:

- (1) If the two mirror lines are perpendicular, then by the *Compositions of Reflections over Intersecting Lines Theorem*, this enacts a rotation by  $\pi$  about their intersection. This populates the  $\mathcal{C}\{(cc)(\sigma\sigma)\}$  conjugacy class. There are 9 such intersections (each entry of the magic square), agreeing with the class's number of elements in Table I.
- (2) If the two mirror lines are parallel, then by the *Reflection in Parallel Lines Theorem*, this enacts a translation normal to the two lines. That is,  $\varphi_2$  translates along either the diagonal or antidiagonal directions of the magic square, and thus belongs to

$\mathcal{C}\{(ccc)(\sigma\sigma\sigma)\}$ . There are two directions and two nontrivial and nonequivalent magnitudes of translation, forming the 4 elements in this class.

There are two more conjugacy classes remaining in the even-parity component:  $\mathcal{C}\{(c\sigma c\sigma c\sigma)\}$  and  $\mathcal{C}\{(ccc)\}$ . We can realize any automorphism in the former class, e.g.  $(c_1\sigma_1c_2\sigma_2c_3\sigma_3)$ , with a sequence  $\{\mathbb{1}, A_1, A_2, A_3\}$  by choosing  $\tau_{32} = (c_1\sigma_3)(c_2\sigma_2)(c_3\sigma_3)$  and  $\tau_{21}\tau_{10} = (c_1c_3)(\sigma_1\sigma_2)$  such that  $\varphi_3 = \tau_{32}\tau_{21}\tau_{10}$ . It is not possible to realize  $\mathcal{C}\{(ccc)\}$  with such a sequence because this class has trivial  $S_2$  components but an odd number of  $\tau$  reflections results in a net nontrivial reflection. Rather, using a sequence  $\{\mathbb{1}, A_1, A_2, A_3, A_4\}$  we can compose a diagonal translation  $\tau_{43}\tau_{32}$  with an antidiagonal translation  $\tau_{21}\tau_{10}$  such that  $\varphi_4 = \tau_{43}\tau_{32}\tau_{21}\tau_{10}$  translates along the vertical or horizontal directions of the magic square, realizing any  $\mathcal{C}\{(ccc)\}$ .<sup>21</sup>

For any two arbitrary FETs in the same component,  $A$  and  $B$ , with associated automorphisms  $\varphi_A$  and  $\varphi_B$ , the minimum graph distance between them can be found by identifying the minimum graph distance between the trivial FET and the FET with automorphism  $\tau_{BA}$ . That is, let the minimum adjacency sequence between  $\mathbb{1}$  and the FET with automorphism  $\tau_{BA}$  be  $\{\mathbb{1}, A_1, \dots, A_{\tau_{BA}}\}$  containing  $m + 1$  FETs. Then by concatenating each of the  $m$  1-component disorder models in this adjacency sequence with the measurement sequence for  $A$ , we get  $\{A, A \cdot A_1, \dots, A \cdot A_{\tau_{BA}} = B\}$  (with  $\cdot$  used informally here to denote the result of concatenating the two measurement sequences of those FETs). There does not exist a shorter adjacency sequence between  $A$  and  $B$ , because if there did then we could perform the reverse process and concatenate each of its FETs with a measurement sequence for  $\varphi_A^{-1}$ , thereby realizing an adjacency sequence between  $\mathbb{1}$  and  $\tau_{BA}$  with less than  $m + 1$  FETs. For example, take  $(rb)$  and  $(rgb)(xy)$ . Their transition map is  $\tau = (rgb)(xy) \cdot (rb)^{-1} = (gb)(xy)$ , which is connected to the trivial FET via a graph distance of 2, and thus the FETs with automorphisms  $(rb)$  and  $(rgb)(xy)$  are also connected via a graph distance of 2.

1-component disorder models therefore prompt a notion of connectivity between FETs of the DA color code. We have seen that two FETs with different parity on the  $S_3 \times S_3$  subgroup cannot be connected in this way, and the minimum length adjacency sequence for two FETs with automorphisms  $\varphi_A$  and  $\varphi_B$  is found by taking the minimum length sequence between the trivial FET and the FET with automorphism  $\tau_{BA}$ . These results will be used

in Section IV C to justify conditions relating the potential automorphisms that can be realized while preserving reversible condensations despite missing measurements.

## B. Logically-Connected FETs

We have so far stated sufficient and necessary conditions on the theoretical ability for disorder to generate different automorphisms and FETs. We now consider the behavior of the systems evolving over multiple periods of these measurement sequences, and whether there exists protected logical qubits that remain unaffected, even near the critical point of  $p \sim p_c$  where logical measurements are expected. In a DA circuit, restricting gates to only those that correspond to the automorphisms of logically-connected FETs helps ensure that logical qubits remain protected even with increasing circuit depth.

In the long-time limit, the number of protected logical qubits supported on a 2-torus will always be even: if an operator  $\tilde{O}[\mathbf{c}]_v$  is measured, the commuting operator  $\tilde{O}[\mathbf{c}]_h$  can also be measured under a different disorder realization in subsequent periods. A code evolving under a particular disorder model will therefore always have 0, 2, or 4 qubits measured out (or conversely, protected) in the limit of  $t \rightarrow \infty$  periods. To quantify which competing automorphisms permit such protected qubits, we introduce a stricter definition of connectedness:

**Definition 3** (Logically-Connected). *Two FETs  $A_0$  and  $A_m$  are logically-connected if there exists an adjacency sequence of FETs  $\{A_0, \dots, A_m\}$  with a consistent nonzero-dimensional logical Hilbert subspace that remains protected in the limit of  $t \rightarrow \infty$  periods, for any  $p \in [0, 1]$  in any of the  $m$  sets of 1-component disorder models between FETs  $A_i$  and  $A_{i+1}$ .*

Here, “consistent” means that the same logical Hilbert subspace is protected in all of the 1-component disorder models; we interpret this as there being a logical qubit that is unaffected by the disorder modifying  $A_0$  into  $A_m$ . By definition, any  $A_i, A_j$  in the sequence are also logically-connected, and logically-connected FETs are necessarily also connected FETs.

We first consider adjacent FETs. Let  $\varphi_A$  and  $\varphi_B$  be the two competing automorphisms. The nontrivial anyon that localizes at  $\tau_{BA} \in \mathcal{C}\{(c\sigma)(c\sigma)(c\sigma)\}$  is a fermion, which braids trivially with itself and the vacuum. From Section III, if all anyons  $\mathbf{c}$  that localize at  $\tau_{BA}$  braid trivially, then each pair of mutual-semions that are invariant under  $\tau_{BA}$  and braid trivially with all  $\varphi_A^{-t}(\mathbf{c})$  for  $t = 0, 1, 2, \dots$  guarantees the existence of 2 protected logical qubits as  $t \rightarrow \infty$ .

This allows us to restrict which automorphisms can be logically-connected; to do so, we first explain how automorphisms map the fermions of the color code. As detailed in Appendix A 1, there are 6 fermions, forming two fermion groups  $F$  and  $F'$  with  $-1$  mutual statistics between different fermions within the same group

<sup>21</sup> We can also show that these are the minimum graph distances between each FET by considering the  $\mathcal{D}^2$  of the conjugacy classes. The reflections  $\mathcal{C}\{(c\sigma)(c\sigma)(c\sigma)\}$  have  $\mathcal{D}^2 = 2$ .  $\mathcal{C}\{(ccc)(\sigma\sigma\sigma)\}$  and  $\mathcal{C}\{(cc)(\sigma\sigma)\}$  have  $\mathcal{D}^2 = 4$ , requiring two reflections to populate a fusion group with the required number of localized anyons. Similarly,  $\mathcal{C}\{(c\sigma c\sigma c\sigma)\}$  has  $\mathcal{D}^2 = 8$  and  $\mathcal{C}\{(ccc)\}$  has  $\mathcal{D}^2 = 16$ , requiring three and four reflections respectively.

and trivial mutual statistics otherwise. These fermions are mapped by automorphisms according to the lemma (proof in Appendix A 1):

**Lemma 2.** *For any fermion  $f$ , if the automorphism  $\varphi$  has even parity on the subgroup  $S_3 \times S_3$ , then the fermion  $\varphi(f)$  is in the same fermion group as  $f$ . If the parity is odd, then  $\varphi(f)$  is in the other fermion group.*

Now, if two fermions are in different fermion groups, there is no fermion that braids trivially with both. Moreover, using the “fermion magic square” from Appendix A 1, a given fermion  $f \in F$  only braids trivially with the bosons in its row (and the vacuum). For example,  $ry \times bx \times gz$  only braids trivially with the  $ry$ ,  $bx$ , and  $gz$  bosons. Similarly,  $f' \in F'$  only braids trivially with the bosons in its column. Therefore, the sole boson that braids trivially with both  $f$  and  $f'$  is the boson at the intersection of the row and column. By Lemma 2, for any fermion  $f$  there thus exists one nontrivial anyon, not a pair of mutual-semions, that braids trivially with both  $f$  and  $\varphi^{-1}(f)$  if  $\varphi$  has odd-parity on  $S_3 \times S_3$  (noting that the parity of  $\varphi$  and  $\varphi^{-1}$  are the same). Hence, two FETs with automorphisms of odd-parity on  $S_3 \times S_3$  cannot be logically-connected. Moreover, since FETs in the odd-parity component are connected only to other FETs in the odd-parity component, this means that they are logically-connected to no FET. Any 1-component disorder model involving an odd-parity FET and tuned near the critical point will necessarily measure out all 4 logical qubits given enough time.

We now consider FETs connected via a sequence of adjacent FETs  $\{A_0, A_1, \dots, A_m\}$  with automorphisms  $\varphi_0, \varphi_1, \dots, \varphi_m$ . If there exists a common protected logical subspace in the 1-component disorder models between each pair of FETs  $A_i$  and  $A_{i+1}$ , then the localized fermion in each case must be from the same fermion group. We note the lemma (proof in Appendix A 1):

**Lemma 3.** *If two reflections  $\tau_1, \tau_2 \in \mathcal{C}\{(c\sigma)(c\sigma)(c\sigma)\}$  are about parallel mirror lines of the magic square, then their localized anyons are fermions in the same fermion group. Otherwise, they are in different fermion groups.*

Therefore, for this condition to hold, each  $\tau_{(i+1)i}$  must be a reflection about a mirror line parallel to all other  $\tau_{(j+1)j}$  in the adjacency sequence, with  $i, j = 0, \dots, m-1$ . By the *Reflection in Parallel Lines Theorem*, the only possible conjugacy classes created from an even number of these reflections are translations along a diagonal of the magic square, that is  $\mathcal{C}\{\text{id}\}$  or  $\mathcal{C}\{(ccc)(\sigma\sigma\sigma)\}$ . An odd number of reflections results in another reflection about a parallel mirror line. Therefore, assuming that  $A_0 \neq A_m$ , a necessary condition for  $A_0$  and  $A_m$  to be logically-connected is that

$$\tau_{m0} \in \mathcal{C}\{(ccc)(\sigma\sigma\sigma)\} \quad (27)$$

for even  $m$ , or

$$\tau_{m0} \in \mathcal{C}\{(c\sigma)(c\sigma)(c\sigma)\} \quad (28)$$

Table II. Protected logical algebra for a localized  $F$ -fermion.

Operator	Anyon Representation	Equivalent Logical
$\tilde{X}_1$	$\bar{O}[rx \times bz]_v$	$\bar{X}_1 \bar{Z}_4$
$\tilde{Z}_1$	$\bar{O}[rz \times by]_h$	$\bar{Z}_1 \bar{Z}_2 \bar{X}_3$
$\tilde{X}_2$	$\bar{O}[rx \times bz]_h$	$\bar{Z}_1 \bar{X}_4$
$\tilde{Z}_2$	$\bar{O}[rz \times by]_v$	$\bar{X}_2 \bar{Z}_3 \bar{Z}_4$

Table III. Protected logical algebra for a localized  $F'$ -fermion.

Operator	Anyon Representation	Equivalent Logical
$\tilde{X}_1$	$\bar{O}[rz \times bx]_v$	$\bar{X}_2 \bar{Z}_3$
$\tilde{Z}_1$	$\bar{O}[rx \times by]_h$	$\bar{Z}_1 \bar{X}_3 \bar{X}_4$
$\tilde{X}_2$	$\bar{O}[rz \times bx]_h$	$\bar{Z}_2 \bar{X}_3$
$\tilde{Z}_2$	$\bar{O}[rx \times by]_v$	$\bar{X}_1 \bar{X}_2 \bar{Z}_4$

for odd  $m$ . Furthermore, we know from Section IV A that if  $\tau_{BA} \in \mathcal{C}\{(c\sigma)(c\sigma)(c\sigma)\}$  then FETs  $A$  and  $B$  are adjacent, and if  $\tau_{BA} \in \mathcal{C}\{(ccc)(\sigma\sigma\sigma)\}$  then FETs  $A$  and  $B$  are connected using two 1-component disorder models. Moreover, in a valid FET with reversible condensations we conjecture that there is no other mechanism for affecting the logical subspace beyond the measured fermions discussed here, and so these conditions should guarantee the existence of a consistent protected non-zero dimensional logical subspace. Assuming this conjecture to be true, any two arbitrary FETs  $A$  and  $B$  are logically-connected iff their automorphisms have even parity on  $S_3 \times S_3$ , and  $\tau_{BA}$  satisfies either Eq. (27) or Eq. (28).

For models where there is a protected logical subspace, these results also enable a prescription to identify representatives of its protected logical operators: for  $S_3 \times S_3$  even-parity automorphisms,  $\varphi^{-t}(f)$  are guaranteed to be in the same fermion group for all integers  $t \geq 0$  by Lemma 2. Therefore, the protected logical operators are constructed out of fermions from the other group, which are guaranteed to braid trivially with all measured fermions. There are thus two possible candidates for logical subspaces that are protected in a 1-component disorder model: if the localized fermion belongs to the  $F$  fermion group, then a representative logical algebra is given by Table II; if it belongs to the  $F'$  fermion group, then we instead use Table III. Because the anyons that construct these protected operators are all invariant under the transition maps between the logically-connected FETs, the time-evolution of an observable from this protected algebra at point  $p \in [0, 1]$  in any logically-connected 1-component disorder model is indistinguishable from any other point  $\tilde{p} \in [0, 1]$ . That is, if two FETs are logically-connected, their automorphisms have the same action on a protected logical qubit.

### C. $m$ -Component Disorder Models

We have so far considered only pairs of FETs that arise from 1-component disorder models. That is, only one stage of the measurement sequence was permitted to have missing measurements. Although this revealed several important insights into the structure of automorphisms in the DA color code, it is ultimately a largely unphysical assumption. We now generalize our results to so-called “ $m$ -component disorder models” where we introduce  $m$  parameters  $p_1, \dots, p_m \in [0, 1]$  that determine the probability of independently measuring links in  $m$  components of the measurement sequence. This allows for more realistic models where more—or all—of the measurement may be randomly included or excluded. For example, a 2-component disorder model with two independent disordered stages and probabilities  $p_1$  and  $p_2$  is

We can associate such a model with a 2-dimensional parameter space  $[0, 1]^2$  indexed by vectors  $\mathbf{p} = (p_1, p_2)$ . The four corners of this parameter space have measurement sequences that enact four different automorphisms:

$p_1$	0	1
$p_2$	id	$(rx)(gy)(bz)$
0	$(rz)(gx)(by)$	$(rgb)(xzy)$
1		

Additional examples of 2-component disorder models are given in Appendix B 1.

What  $m$ -component disorder models do not contain any measurement sequences with irreversible condensations? Or, conversely, what models must contain irreversible condensations? We saw in Section IV A that two FETs with automorphisms of different parity on  $S_3 \times S_3$  cannot be connected. If an  $m$ -component disorder model realizes two such automorphisms, then corners of the parameter space must host a measurement sequence with irreversible condensations (otherwise, we could construct several 1-component disorder models using pairs of FETs in adjacent corners that connect the two different-

parity FETs). For example, consider the following:

The corners of the 2-dimensional parameter space are furnished by

$p_1$		0		1	
$p_2$					
0	$(rz)(gx)(by)$		$\text{IrrP}$		
1		$\text{IrrP}$	$(rybz)(gx)$		

containing two FETs with automorphisms of different parity on  $S_3 \times S_3$ , and two phases with interlayer irreversible condensations indicated by “IrrP”. Such models, when tuned near the critical lines of  $p_i \sim p_c$ , will feature semi-punctures that irreversibly remove logical information from the system. An  $m$ -component disorder model that realizes automorphisms with differing  $S_3 \times S_3$  parities will therefore not have protected logical subspaces. If we take every stage in a measurement sequence to be disordered, then this tells us that if one of the automorphisms has odd-parity on  $S_3 \times S_3$ , there must be irreversible condensations somewhere in the parameter space. This is because if every stage is disordered, then the trivial FET with  $\widetilde{CC} \rightarrow \widetilde{CC}$  exists in the parameter space, and  $\text{id}$  has even parity.

We can also consider a stronger criterion: what disorder models are possible that retain a nonzero-dimensional protected logical subspace? From Section IV B, two FETs that are logically-connected must satisfy Eq. (27) or Eq. (28). If these FETs populate corners of the  $m$ -dimensional parameter space for an  $m$ -component disorder model, this now enables not only  $\tau_{BA} \in \mathcal{C}\{(c\sigma)(c\sigma)(c\sigma)\}$  domain walls, but by Eq. (27) also  $\tau_{CA} \in \mathcal{C}\{(ccc)(\sigma\sigma\sigma)\}$  when  $p_i \notin \{0, 1\}$  for at least two coordinates. These  $\tau_{CA}$  boundaries have  $\log_2 \mathcal{D}^2 = 2$ ; the nontrivial anyons that localize are the three fermions from one of the  $F$  or  $F'$  groups, and the protected logical algebra is again given by either Table II or III. If there does not exist a consistent logically-protected subspace, then there must exist  $\tau$  in other conjugacy classes with  $\log_2 \mathcal{D}^2 > 2$ ; anyons beyond the three fermions in  $F$  or  $F'$  are measured and  $\text{IMS} = 0$ . This is consistent with  $\mathcal{C}\{(c\sigma)(c\sigma)(c\sigma)\}$  and  $\mathcal{C}\{(ccc)(\sigma\sigma\sigma)\}$  being the sole (nontrivial) conjugacy classes with automorphisms that have invariant mutual-semion pairs. In order for an  $m$ -component disorder model to have a consistent logically-protected subspace at all values of its  $m$ -dimensional parameter space, we require that:

- (1) all corners of the hypercube in parameter space are FETs consisting of reversible sequences of condensations;
- (2) the enacted automorphisms have even parity on the subgroup  $S_3 \times S_3$ ; and
- (3) all pairs of FETs satisfy Eq. (27) if their locations differ by an even Manhattan distance,<sup>22</sup> or Eq. (28) if an odd Manhattan distance.

An immediate—and intuitive—consequence of these criteria is that if every anyon condensation in a measurement sequence is disordered, then if there exists a protected logical subspace, those logical operators do not evolve under any of the involved automorphisms. This is because the trivial automorphism  $\text{id}$  is in the parameter space, and all automorphisms act equivalently on the protected subspace. It is thus not possible to construct a DA color code that implements an automorphism yielding a nontrivial gate while being completely protected against missing measurements. As we show in Appendix C, however, in the thermodynamic limit logical information is measured only once  $p$  approaches a critical point, dependent on the particular disorder model. For 1-component models, we get  $p_c \sim 0.346\dots$  consistent with the universality class of bond percolation on a triangular lattice. This allows for some flexibility in the construction of disorder-resistant DA color codes.

Analyzing missing measurements via competing automorphisms reveals key structure about the effects of disorder in the DA color code. Given a sequence of anyon condensations (or link measurements) for an FET, by identifying the automorphisms created when stages are omitted, one can immediately read off whether logical qubits are measured or protected due to the disorder. We have shown necessary conditions for disorder models to support a 2-qubit logical subspace that is entirely immune to the disorder. In these cases, at any point in the  $m$ -dimensional parameter space, the time-evolution of protected logical operators will be independent of the disorder realizations. These results therefore may help determine—or rule-out—feasible implementations and measurement sequences for disorder-resistant DA color codes.

## V. CONCLUSIONS AND OUTLOOK

Spatiotemporally heterogeneous domain walls naturally introduce disorder to measurement-induced Floquet-enriched topological orders. We analyzed the evolution and purification dynamics of the degenerate codespace amid this heterogeneity—or “competing automorphisms”. We showed that this behavior is agnostic to

microscopic details and is directly determined by TQFT features: anyon braiding and fusion properties (the modular data of the Abelian TO) and the properties of the involved automorphisms.

Interpreting these systems as topological stabilizer codes, the number of independent nontrivial anyons that localize at the domain wall boundaries determines the number of nontrivial logical operators that may undergo measurement during one period of competition. For a  $\mathbb{Z}_2$ -based TO, this equals  $\log_2 \mathcal{D}^2$ , where  $\mathcal{D}$  is the quantum dimension of the twist associated to the transition map between the neighboring automorphisms. In these systems, the number of mutual-semions that are invariant under this transition map,  $\text{IMS}$ , indicates the number of logical qubits that are protected from any such logical measurement over one period. For a code with  $k$  logical qubits, these properties satisfy  $\log_2 \mathcal{D}^2 + \text{IMS} \leq k$ . For a  $CC$  topological order, Table I shows these values for all conjugacy classes of its automorphism group  $\text{Aut}[CC]$ .

This new understanding of disordered FETs enables us to readily discern the effects that missing-measurement noise models or perturbations to measurement sequences have on dynamical codes such as the DA color code [32]. The regions subjected to missing measurements in a given random realization are precisely the heterogeneous temporal domain walls in an FET with competing automorphisms.  $\log_2 \mathcal{D}^2$  and  $\text{IMS}$  are thus key metrics that characterize the ability for a given noise model to result in logical measurements and the number of logical qubits that remain protected.

We first established results for models with only one measurement stage disordered, before generalizing to multiple or  $m$ -component disorder models. We argued that it is not possible to construct a measurement sequence where every stage is disordered while simultaneously maintaining a consistent protected logical subspace and nontrivial effect of automorphisms on logical operators in this subspace. Implementations of the DA color code must therefore take into account the effects of missing measurements. We show, nevertheless, in Appendix C, that even where a logical subspace is not immune across the entire parameter space, if the noise level is below a critical value then information can still be protected. In this scenario, it would be beneficial for such a code to not result in irreversible condensations in its measurement sequence. We showed that this is only possible throughout the entire parameter space if the enacted automorphisms have even parity on the subgroup  $S_3 \times S_3$ . In practice, the occurrence of irreversible condensations may be detected, and the realized measurement sequences can be post-selected by discarding those that result in a loss of encoded information.

Our perspective of competing automorphisms has allowed us to chart the topology of the parameter space of DA color code FETs. For example, two FETs,  $A$  and  $B$  with automorphisms  $\varphi_A$  and  $\varphi_B$ , can compete using a disorder model with one random measurement stage (a “1-component disorder model”) if and

<sup>22</sup> The Manhattan distance is the sum of the component-wise (absolute) differences between two  $\mathbf{p}$  vectors.

only if the transition map  $\varphi_B \varphi_A^{-1}$  is in the conjugacy class  $\mathcal{C}\{(c\sigma)(c\sigma)(c\sigma)\}$  of automorphisms that reflect the anyons of the color code magic square about a diagonal mirror line. We presented additional conditions that restrict the ability for two competing automorphisms to support a consistent nonzero-dimensional logical subspace that remains unmeasured over multiple periods. This allows one to better understand the behavior of a given measurement sequence, and how it may be modified or corrupted by possible missing measurements.

Important open questions remain about disorder in the DA color code, such as the interplay between competing automorphisms and open boundaries or lattice defects [20, 25]. It remains to be seen how the effectiveness of the code's error-correction capabilities (such as the existence of a threshold, fault-tolerance, or decoders) is affected by competing automorphisms. Future work should also consider the effect of more general disorder models, such as with weak measurements [15, 16], interspersed random unitaries [54], coherent errors [90], or single-qubit measurements [35, 48, 91]. We expect our perspective of competing automorphisms to be potentially useful in any disorder model that realizes spatiotemporally heterogeneous domain walls.

Moving beyond the DA color code, this work is a first step towards understanding general dynamical TOS that can support multiple automorphisms. Although we focused on FETs on a 2-torus, our results are readily generalizable to other manifolds by considering their noncontractible cycles. Future works could investigate other TOS, including microscopic models for those with Abelian anyons beyond mutual-semions, and general features of competing automorphisms in non-Abelian anyon theories [69, 92] or fracton Floquet phases [78, 93]. It would be also interesting to study what competing automorphisms can reveal about FETs evolving under unitary dynamics instead of measurements [30, 31, 78].

## ACKNOWLEDGMENTS

This research was supported by the Gates Cambridge Trust and by EPSRC grant EP/V062654/1.

## Appendix A: Additional Background Material

### 1. Color Code Fermions

In the color code, there are 6 fermions. These can be written as a unique fusion product of three mutual-semions:

$$\begin{array}{ll} \underbrace{\mathbf{ry} \times \mathbf{bx} \times \mathbf{gz}}_F & \underbrace{\mathbf{ry} \times \mathbf{bz} \times \mathbf{gx}}_{F'} \\ \underbrace{\mathbf{bz} \times \mathbf{gy} \times \mathbf{rx}}_F & \underbrace{\mathbf{bx} \times \mathbf{gy} \times \mathbf{rz}}_{F'} \\ \underbrace{\mathbf{gx} \times \mathbf{rz} \times \mathbf{by}}_F & \underbrace{\mathbf{gz} \times \mathbf{rx} \times \mathbf{by}}_{F'} \end{array} \quad (A1)$$

The fermions form two groups,  $F$  and  $F'$ . Fermions within  $F$  are mutual-semions with fermions from  $F$  and braid trivially with those from  $F'$ , and vice versa. These products can also be summarized in the fermion magic square [32]:

$$F \left\{ \begin{array}{|c|c|c|} \hline \mathbf{ry} & \mathbf{bx} & \mathbf{gz} \\ \hline \mathbf{bz} & \mathbf{gy} & \mathbf{rx} \\ \hline \mathbf{gx} & \mathbf{rz} & \mathbf{by} \\ \hline \end{array} \right. \underbrace{\quad}_{F'} \quad (A2)$$

such that the product of the three anyons in a row or column give fermions in  $F$  and  $F'$  respectively. In contrast to the magic square [cf. Eq. (2)] where anyons in the same row or column braid trivially, anyons in the same row or column of the fermion magic square are mutual-semions. Anyons not sharing a row or column braid trivially. These fermions can also be (non-uniquely) formed from the fusion of just two mutual-semions:

$$\begin{aligned} \mathbf{gx} \times \mathbf{bz} &\equiv \mathbf{gy} \times \mathbf{rz} \equiv \mathbf{rx} \times \mathbf{by} \\ \mathbf{bx} \times \mathbf{rz} &\equiv \mathbf{by} \times \mathbf{gz} \equiv \mathbf{gx} \times \mathbf{ry} \\ \mathbf{rx} \times \mathbf{gz} &\equiv \mathbf{ry} \times \mathbf{bz} \equiv \mathbf{bx} \times \mathbf{gy} \\ &\underbrace{\quad}_{F} \\ \mathbf{bx} \times \mathbf{gz} &\equiv \mathbf{by} \times \mathbf{rz} \equiv \mathbf{rx} \times \mathbf{gy} \\ \mathbf{rx} \times \mathbf{bz} &\equiv \mathbf{ry} \times \mathbf{gz} \equiv \mathbf{gx} \times \mathbf{by} \\ \mathbf{gx} \times \mathbf{rz} &\equiv \mathbf{gy} \times \mathbf{bz} \equiv \mathbf{bx} \times \mathbf{ry} \\ &\underbrace{\quad}_{F'} \end{aligned} \quad (A3)$$

In the main text, we stated a lemma about whether the groups  $F$  and  $F'$  are closed under automorphisms. We provide a proof of this lemma now:

*Proof of Lemma 2.* The automorphism that is trivial on  $S_3 \times S_3$  and nontrivial on  $S_2$  is the color-flavor reflection  $(rx)(gy)(bz)$ . On the fermion magic square [Eq. (A2)], this automorphism acts as a reflection about a horizontal mirror line through  $\mathbf{rx}$ ,  $\mathbf{gy}$ , and  $\mathbf{bz}$ ; this reflection does not change the fermion group. It is therefore sufficient to examine the action only on the  $S_3 \times S_3$  component of an automorphism. We first consider the simplest such nontrivial automorphisms, the 2-cycles  $(cc)$  or  $(\sigma\sigma)$ . These act as a reflection on the fermion magic square about diagonal or antidiagonal mirror lines (considering the square on a 2-torus). A fermion in  $F$  thus maps to one in  $F'$  and vice versa as the rows and columns are interchanged. Any general even-parity (odd-parity) permutation is an even (odd) product of 2-cycles, swapping  $F$  and  $F'$  an even (odd) number of times. Therefore, the even-parity  $S_3 \times S_3$  automorphisms do not swap  $F$  and  $F'$ , while odd-parity automorphisms do.  $\square$

We also stated a lemma on the localized anyons for parallel reflections in  $\mathcal{C}\{(c\sigma)(c\sigma)(c\sigma)\}$ . We provide the proof here:

*Proof of Lemma 3.* If two automorphisms  $\tau_1, \tau_2 \in \mathcal{C}\{(c\sigma)(c\sigma)(c\sigma)\}$  are equal, then their localized anyons are the same. If they are unequal, consider the case where we can interpret them geometrically as reflections about inequivalent but parallel lines of the magic square (on a 2-torus). Their mirror lines do not intersect, and their constituent 2-cycles ( $c\sigma$ ) are all different (since the mirror line for  $(c_1\sigma_1)(c_2\sigma_2)(c_3\sigma_3)$  is precisely the line through anyons  $c_1\sigma_1$ ,  $c_2\sigma_2$  and  $c_3\sigma_3$ ). Moreover, the product of these three anyons— $c_1\sigma_1 \times c_2\sigma_2 \times c_3\sigma_3$ —is precisely the fermion that localizes at the twist for the automorphism. Therefore, the two fermions that localize at  $\tau_1$  and  $\tau_2$  respectively occupy distinct rows (or columns) of the fermion magic square, and are thus in the same fermion group. On the other hand, if the automorphisms have perpendicular mirror lines, then their  $c\sigma$  labels intersect at some point on the magic square such that the localized fermions have one shared label, and thus are in different fermion groups.  $\square$

## 2. Group Theory

### a. Group Theory Essentials

In this section we briefly outline some ideas from group theory that are relevant for our discussions of the automorphism group in Appendix A 2b.

We first outline general group properties, starting with group products. For a group  $G$ , a subgroup  $N \triangleleft G$  is normal if and only if  $gng^{-1} \in N$  for all  $g \in G$  and  $n \in N$ . That is, elements of  $N$  are invariant under conjugation by all elements of  $G$ , or equivalently the left and right cosets  $gN$  and  $Ng$  are equal for all  $g \in G$ . When  $G$  is a semidirect product, written as  $G = N \rtimes H$ , and where  $N$  is normal in  $G$  but  $H$  may not be, then for every  $g \in G$ , there are unique  $n \in N$  and  $h \in H$  such that  $g = nh$ .

For a group  $G$  and two elements  $a, b \in G$ , if  $b = gag^{-1}$  for some  $g \in G$ , then  $a$  and  $b$  are conjugate. Conjugacy is an equivalence relation that partitions  $G$  into conjugacy classes, denoted as

$$\mathcal{C}_a = \{gag^{-1} \mid g \in G\} \quad (\text{A4})$$

for some representative  $a \in G$ . All elements belonging to the same conjugacy class have the same order, the minimal  $k$  such that  $a^k = \text{id}$ .

We now consider specifically the permutation group,  $S_n$ , which is the group of re-orderings of a set of  $n$  elements. We write these permutations using cycle notation. For example, labelling the  $n$  elements as  $a, b, \dots, n$ , the permutation  $(ade)(fg)$  indicates the map  $a \mapsto d \mapsto e \mapsto a$ ,  $f \mapsto g \mapsto f$ , with the other elements unchanged. A cycle is a closed mapping, such as  $(ade)$  or  $(fg)$ . The order (or length) of a cycle can be read off as the number of elements listed; a cycle of length  $k$  is called a  $k$ -cycle.  $(ade)$  is a 3-cycle, for example. A cycle is defined as having even (odd) parity if it can be written as an even

(odd) number of 2-cycles. For example,  $(ade) = (ad)(de)$  and therefore is even parity. Equivalently, a  $k$ -cycle is even (odd) if  $k - 1$  is even (odd). A permutation can be written in multiple ways:  $(ade)(fg)$  is the same as  $(gf)(dea)$ . However, the number and lengths of disjoint cycles forming a permutation are a fixed property of that permutation [94]. The “cycle type” of a permutation is written in bracket notation as

$$[1^{\alpha_1} 2^{\alpha_2} \cdots n^{\alpha_n}] \quad (\text{A5})$$

where  $\alpha_k$  is its number of disjoint  $k$ -cycles. For example,  $(ade)(fg)$  has cycle type  $[2^1 3^1]$  (with  $\alpha_0 = 0$  omitted for brevity). Notably, the conjugacy classes of a permutation group are characterized by its elements all having the same cycle type [94].

### b. Automorphism Group Essentials

In this section we apply the previous group-theory ideas to the automorphism group of the color code,  $\text{Aut}[CC]$ . Concretely,  $\text{Aut}[CC]$  is the group of permutations of the anyons of the color code that preserve the relationships and structure of the anyons. That is, mutual-statistics, self-statistics, and fusion rules must remain equivalent after applying  $\varphi \in \text{Aut}[CC]$  to all anyons. We can represent any automorphism by a relabelling of the 6 color and flavor labels,  $r, g, b, x, y, z$ , since all  $c$ -colored or  $\sigma$ -flavored anyons must transform equally in order to maintain their mutual statistics and fusion rules.  $\text{Aut}[CC]$  is therefore a subgroup of  $S_6$ . We represent its elements using cycle notation, such as  $(rbg)(xy)$ . When color and flavor are interchanged, we have cycles such as  $(rxgy)(bz)$ ; although the standalone map  $r \mapsto x$  is ill-defined, the construction of each anyon in terms of both a color and a flavor ensures that as long as all the cycles either alternate colors and flavors, or have disjoint color-only and flavor-only cycles, the anyon mapping is valid. This cycle, for example, maps  $rx \mapsto gx$  as  $r \mapsto x$ ,  $x \mapsto g$ . A cycle such as  $(rxg)$  is not in  $\text{Aut}[CC]$  for this reason.

As with the permutation groups,  $\text{Aut}[CC]$  can be partitioned into conjugacy classes; Table I lists the 9 conjugacy classes and their cycle types. These are subsets of the  $S_6$  conjugacy classes and are generated by and closed under conjugation with elements from  $\text{Aut}[CC]$ .

Automorphisms in  $\text{Aut}[CC]$  can be identified by the decomposition into subgroups  $(S_3 \times S_3) \rtimes S_2$ , representing the  $S_3$  group of 3! color (magic square row) permutations, the  $S_3$  group of 3! flavor (magic square column) permutations, and the  $S_2$  group of 2 color-flavor exchanges [26, 32]. Specifically, the  $S_2$  corresponds to a reflection about the mirror line through the  $rx - gy - bz$  diagonal. In cycle notation, the nontrivial element of  $S_2$  [with trivial  $(S_3 \times S_3)$  contribution] is  $(rx)(gy)(bz)$ .  $(S_3 \times S_3)$  is closed under conjugation and hence is a normal subgroup.  $S_2$ , on the other hand, is not. For example,

$$(rb) \cdot (rx)(gy)(bz) \cdot (rb)^{-1} = (rz)(gy)(bx). \quad (\text{A6})$$

Hence, we use the semidirect product  $\rtimes$ . To identify whether an element has nontrivial  $S_2$  contribution, we note that for this there must be alternating color-flavor labels in the cycle notation:  $(rbg)(xy)$  is trivial on  $S_2$  while  $(rxybygz)$  is not.

An important concept in Section IV A is the parity of an automorphism on the subgroup  $(S_3 \times S_3)$ . To identify this, we first trivialize any  $S_2$  contribution by composing the automorphism with  $(rx)(gy)(bz)$  if it has alternating color-flavor labels. We then multiply the parity of the resulting automorphism's disjoint cycles. For example,  $(ry)(gz)(bx)$  involves a color-flavor reflection and therefore we modify it by

$$(rx)(gy)(bz) \cdot (ry)(gz)(bx) = (rgb)(xzy), \quad (\text{A7})$$

which results in a  $[3^2]$  automorphism with net even  $\times$  even = even parity.<sup>23</sup> Table I lists these parities for all conjugacy classes of  $\text{Aut}[CC]$ .

### 3. Localized Anyons

In Section III, we introduced the notion of localized anyons around the boundaries or twists of domain walls. Lemma 1 was used to determine the presence of operators that are protected during an evolution under multiple temporal domain walls. We prove that lemma here:

*Proof of Lemma 1.* We first show that if  $\mathbf{b} = \tau(\mathbf{b})$  for some automorphism  $\tau$  and anyon  $\mathbf{b}$ , then  $\mathbf{b}$  braids trivially with all  $\mathbf{c}$  that localize at  $\tau$ . For any such anyon  $\mathbf{c}$  that localizes, there exists an  $\mathbf{a}$  such that  $\mathbf{c} = \mathbf{a} \times \tau(\bar{\mathbf{a}})$ . Now, the composite anyon  $\mathbf{a} \times \bar{\mathbf{a}}$  is equivalent to the vacuum 1, and therefore it braids trivially with  $\mathbf{b}$ . We can write this as

$$\exp(2i\theta_{\mathbf{b},\mathbf{a}}) \exp(2i\theta_{\mathbf{b},\bar{\mathbf{a}}}) = 1 \quad (\text{A8})$$

where  $\exp(2i\theta_{\mathbf{a},\mathbf{b}})$  encodes the phase factor accumulated when clockwise encircling an  $\mathbf{a}$  with  $\mathbf{b}$  (or vice versa):

$$(A9)$$

<sup>23</sup> Equivalently, it can be written as an even number of 2-cycles,  $(rg)(gb)(xz)(zy)$

Since  $\tau$  is an automorphism, it preserves these mutual statistics and so

$$\begin{aligned} 1 &= \exp(2i\theta_{\mathbf{b},\mathbf{a}}) \exp(2i\theta_{\tau(\mathbf{b}),\tau(\bar{\mathbf{a}})}) \\ &= \exp(2i\theta_{\mathbf{b},\mathbf{a}}) \exp(2i\theta_{\mathbf{b},\tau(\bar{\mathbf{a}})}) \\ &= \exp(2i\theta_{\mathbf{b},\mathbf{a} \times \tau(\bar{\mathbf{a}})}) \\ &= \exp(2i\theta_{\mathbf{b},\mathbf{c}}) \end{aligned} \quad (\text{A10})$$

where we used  $\mathbf{b} = \tau(\mathbf{b})$  and that  $2(\theta_{\mathbf{b},\mathbf{a}} + \theta_{\mathbf{b},\tau(\bar{\mathbf{a}})})$  is the phase accumulated by  $\mathbf{b}$  encircling  $\mathbf{a} \times \tau(\bar{\mathbf{a}}) = \mathbf{c}$ . Hence, invariant anyons of  $\tau$  braid trivially with all localized anyons of  $\tau$ .

We next prove the reverse direction: any anyon  $\mathbf{b}$  that braids trivially with all localized anyons must be invariant. For any anyon  $\mathbf{a}$ , the anyon  $\mathbf{c} = \mathbf{a} \times \tau(\bar{\mathbf{a}})$  localizes at automorphism  $\tau$ , and therefore  $\mathbf{b}$  braids trivially with  $\mathbf{c}$ :

$$\exp(2i\theta_{\mathbf{b},\mathbf{c}}) = 1. \quad (\text{A11})$$

We again use the statistics-preserving property of automorphisms to write

$$\begin{aligned} 1 &= \exp(2i\theta_{\mathbf{b},\mathbf{a}}) \exp(2i\theta_{\mathbf{b},\tau(\bar{\mathbf{a}})}) \\ &= \exp(2i\theta_{\mathbf{b},\mathbf{a}}) \exp(2i\theta_{\tau^{-1}(\mathbf{b}),\bar{\mathbf{a}}}). \end{aligned} \quad (\text{A12})$$

By anyons and anti-anyons having the same mutual-statistics,  $\theta_{\mathbf{p},\mathbf{q}} = \theta_{\bar{\mathbf{p}},\bar{\mathbf{q}}}$ , we have

$$\begin{aligned} 1 &= \exp(2i\theta_{\mathbf{b},\mathbf{a}}) \exp(2i\theta_{\tau^{-1}(\bar{\mathbf{b}}),\mathbf{a}}) \\ &= \exp(2i\theta_{\mathbf{b},\mathbf{a}}) \end{aligned} \quad (\text{A13})$$

where  $\mathbf{d} = \mathbf{b} \times \tau^{-1}(\bar{\mathbf{b}})$ . This relation holds for all anyons  $\mathbf{a}$ , meaning that there is no anyon encircling action that can distinguish  $\mathbf{d}$  from the vacuum 1 ( $\mathbf{d}$  is “transparent” [61]). For modular anyon theories, such as those formed by topological stabilizer codes, braiding is nondegenerate [64, 69], which implies that  $\mathbf{d}$  is the vacuum. That is,  $\mathbf{b} = \tau^{-1}(\mathbf{b})$  or equivalently,  $\tau(\mathbf{b}) = \mathbf{b}$  as required.  $\square$

### 4. Computing and Creating Automorphisms

Given a dynamical scheme of the form  $\widetilde{CC} \rightarrow TC \boxtimes TC \rightarrow \dots \rightarrow TC \boxtimes TC \rightarrow \widetilde{CC}$ , we compute the enacted automorphism by the formula [32]

$$\varphi_f[(rx)(gy)(bz)]^\alpha [(rz)(gy)(bx)]^\beta \varphi_i^{-1} \quad (\text{A14})$$

where  $\varphi_i$  and  $\varphi_f$  are the contributions from the  $\widetilde{CC} \rightarrow TC \boxtimes TC$  and  $TC \boxtimes TC \rightarrow \widetilde{CC}$  transitions respectively. Table A.1 lists these for all possible reversible transitions.  $\alpha$  is the number of reversible transitions that the first  $CC$  layer undergoes.  $\beta$  is the number of reversible transitions that the second  $CC$  layer undergoes.

For example, consider

$$\begin{array}{c} \widetilde{CC} \rightarrow \begin{array}{|c|c|} \hline 1 & \\ \hline 2 & \\ \hline \end{array} \rightarrow \begin{array}{|c|c|} \hline & 1 \\ \hline & \\ \hline \end{array} \rightarrow \begin{array}{|c|c|} \hline 1 & \\ \hline & 2 \\ \hline \end{array} \rightarrow \widetilde{CC}. \end{array} \quad (\text{A15})$$

Table A.1. All possible isomorphism contributions from the  $\widetilde{CC} \leftrightarrow TC \boxtimes TC$  reversible transitions of a dynamical scheme. Adapted from Ref. 32. There are two possible  $TC \boxtimes TC$  theories for each isomorphism.

Isomorphism	Theories	Isomorphism	Theories
$\text{id}$		$(xy)$	
$(rg)$		$(rg)(xy)$	
$(gb)$		$(gb)(xy)$	
$(rb)$		$(rb)(xy)$	
$(rgb)$		$(rgb)(xy)$	
$(rbg)$		$(rbg)(xy)$	

We have that  $\varphi_i = (gb)$ ,  $\varphi_f = (xy)$ ,  $\alpha = 2$ , and  $\beta = 1$ .  $\alpha$  and  $\beta$  are important only mod 2, since they exponent 2-cycles. This gives overall automorphism

$$(xy) \cdot \text{id} \cdot (rz)(gy)(bx) \cdot (gb)^{-1} = (rz)(gy)(bx). \quad (\text{A16})$$

On the other hand, given any automorphism  $\varphi \in \text{Aut}[CC]$ , it is possible to create a measurement sequence that realizes it. All 72 automorphisms and example measurement sequences are given in Ref. 32. Moreover, it is possible to ensure that this measurement sequence ends with a particular  $TC \boxtimes TC$  condensation prior to returning to  $\widetilde{CC}$ .

We summarize here the procedure described in Ref. 32. Let  $\mathcal{B}_1, \dots, \mathcal{B}_n$  be a sequence of  $n$  sets of bosons of  $CC \boxtimes CC$  that form the condensations for  $n$  child theories  $C_1, \dots, C_n$ . We set  $\mathcal{B}_n = \{1, \mathbf{rz}_1 \mathbf{rz}_2, \mathbf{gz}_1 \mathbf{gz}_2, \mathbf{bz}_1 \mathbf{bz}_2\}$  such that  $C_n = \widetilde{CC}$ . We require that the sequence of condensations is reversible. This allows us to associate an isomorphism  $\lambda$  from  $C_1$  to  $C_n$ . Let  $\phi \in \text{Aut}[CC \boxtimes CC]$  be an automorphism of the parent theory such that  $\phi(\mathcal{B}_1) = \mathcal{B}_1$  and  $\phi(\mathcal{B}_n) = \mathcal{B}_n$ . This also defines an automorphism on  $C_1$  and  $C_n$ ; assume we have chosen  $C_1$  such that  $\phi$  acts as the trivial automorphism  $\text{id}_1$  on  $C_1$ . On  $C_n$  it acts as  $\varphi \in \text{Aut}[CC]$ . The sequence of reversible condensations  $\phi(\mathcal{B}_1), \dots, \phi(\mathcal{B}_n)$  now enacts the isomorphism  $\varphi\lambda$  from  $C_1$  to  $C_n$ . The sequence

$$\mathcal{B}_n, \mathcal{B}_{n-1}, \dots, \mathcal{B}_1, \phi(\mathcal{B}_2), \dots, \phi(\mathcal{B}_{n-1}), \mathcal{B}_n \quad (\text{A17})$$

therefore enacts the automorphism  $\varphi\lambda\lambda^{-1} = \varphi$  on  $C_n = \widetilde{CC}$ . This allows us to create any automorphism  $\varphi \in \text{Aut}[CC]$ .

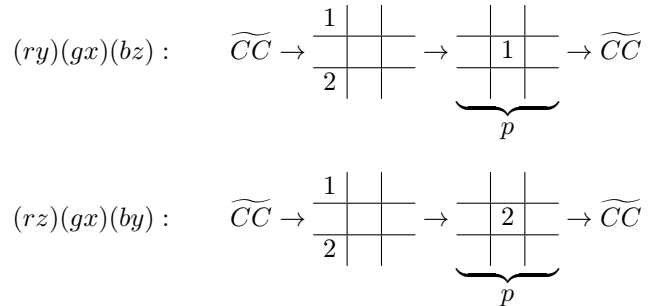
Because  $\lambda$  does not affect the final automorphism, we can arbitrarily specify that  $\mathcal{B}_{n-1}$  is any set of bosons as long as it creates a reversible pair of condensations with  $\widetilde{CC}$  (i.e. any of the theories in Table A.1). If we wish to end with a specific (valid)  $TC \boxtimes TC$  theory with condensed bosons  $\mathcal{B}$ , we therefore specify that  $\mathcal{B}_{n-1} = \phi^{-1}(\mathcal{B})$ . Note that this reasoning allows us to specify only the ending or the first  $TC \boxtimes TC$  theory, not both.

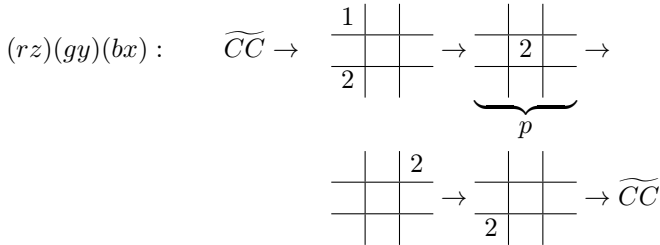
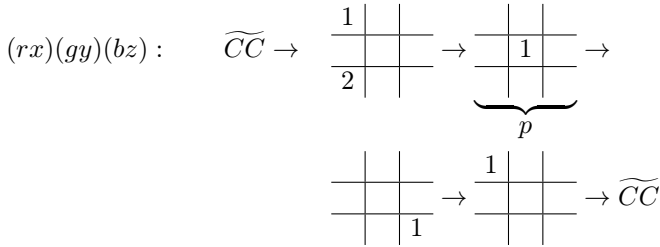
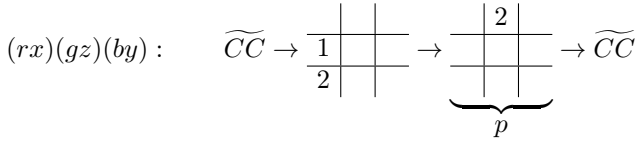
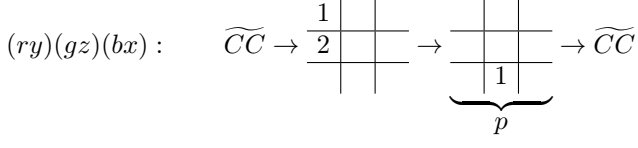
## Appendix B: Disordered DA Color Code

### 1. Example Disorder Models

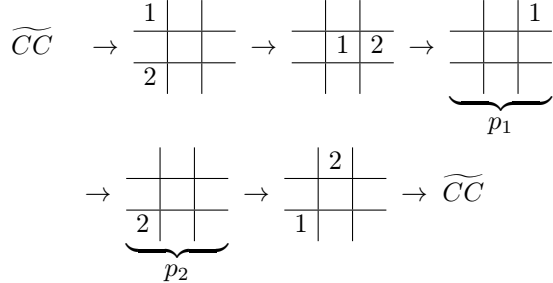
In this section, we provide more examples of disorder models.

*a. Trivial-adjacent FETs* We first consider examples of 1-component disorder models that realize connections between the trivial FET (when  $p = 0$ ) and each of the 6 automorphisms in  $\mathcal{C}\{(c\sigma)(c\sigma)(c\sigma)\}$  (when  $p = 1$ ):





b. *Example 2.* Secondly, consider



with the corners of the parameter space supporting FETs with automorphisms

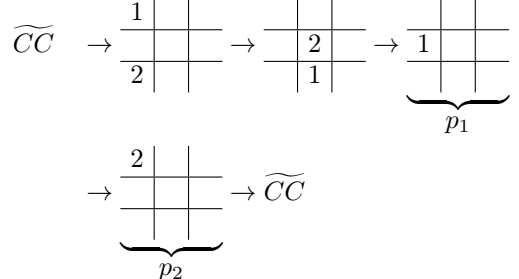
$p_1$	0	1
$p_2$	$(rb)(xy)$	$(rygzbz)$
0	$(rzbygx)$	$(xzy)$
1		

Notably, there does not exist a logically-protected trajectory between  $\mathbf{p} = (0,0)$  and  $\mathbf{p} = (1,1)$  because

$$(xzy) \cdot [(rb)(xy)]^{-1} = (rb)(yz) \notin \mathcal{C}\{(ccc)(\sigma\sigma\sigma)\} \quad (\text{B1})$$

in violation of Eq. (27).

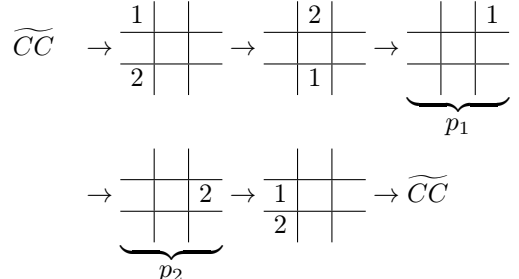
c. *Example 3.* This is an example of a 2-component disorder model where we have an irreversible phase in one corner, from an interlayer irreversible condensation. This differs from Eq. (31) in that all other FETs are in the same parity cluster.



The corners host FETs with automorphisms

$p_1$	0	1
$p_2$	$(rg)(xz)$	$\text{IrrP}$
0	$(rygzbz)$	
1		

d. *Example 4.* This measurement sequence demonstrates multiple automorphisms in the even-parity component; these are connected but cannot be logically-connected.

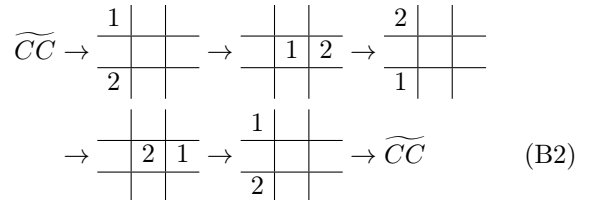


The automorphisms are

$p_1$	0	1
$p_2$	$(rg)$	$(rxgy)(bz)$
0	$(rzgy)(bx)$	
1		

## 2. Connected FETs

We first provide an example of two measurement sequences that both realize the same FET and automorphism,  $\text{id}$ , but are not “connected” to each other: one sequence cannot be made into the other by adding or removing condensation steps and while maintaining solely reversible transitions. The two sequences are



and

$$\widetilde{CC} \rightarrow \begin{array}{|c|c|} \hline 1 & \\ \hline 2 & \\ \hline \end{array} \rightarrow \widetilde{CC}. \quad (\text{B3})$$

Let us begin with Eq. (B2) and consider for now just the first layer. We wish to add or remove condensed bosons to manipulate it into the form of Eq. (B3). The sequence of bosons  $rx, gy, bx, gz, rx$  forms a path on the fermion magic square (the path can wrap around periodic boundary conditions) [32]:

$$\begin{array}{c|c|c|c} ry & bz & z \\ \hline bz & gz & x \\ \hline gx & rz & by \end{array} \quad (\text{B4})$$

The requirement for reversible transitions (that adjacent bosons in the sequence are mutual-semions) necessitates that these arrows only point horizontally or vertically; we must follow this rule when adding or removing condensed bosons. As such, we are never able to remove bosons that sit at the corners of the path—this would result in a diagonal arrow. We may add or remove bosons from the start or end of the sequence only if the resulting pair of layer-1 and layer-2 bosons creates a reversible transition to  $\widetilde{CC}$ ; the  $gz$  boson can never begin or end the sequence. We therefore cannot remove  $gz$  from our sequence. The same argument applies to the sequence of bosons in the second layer. It is thus impossible to connect the measurement sequence of Eq. (B2) with Eq. (B3) while maintaining reversible transitions.

Furthermore, we can also show that not every length- $m$  adjacency sequence can be made into an  $m$ -component disorder model. We discuss here one such example.

Consider the adjacency sequence  $\{A_0, \mathbb{1}, A_2\}$ , where  $\mathbb{1}$  is the trivial FET with automorphism  $\text{id}$ , and  $A_0$  and  $A_2$  have automorphisms  $\varphi_0$  and  $\varphi_2 \in \mathcal{C}\{(\text{c}\sigma)(\text{c}\sigma)(\text{c}\sigma)\}$  respectively [as required by the separation condition, Eq. (23)]. We wish to show that for some choice of  $A_0$  and  $A_2$  there is no 2-component disorder model that realizes  $A_0$ ,  $\mathbb{1}$ , and  $A_2$  in three of its parameter-space corners. Equivalently, there is no measurement sequence  $\widetilde{CC} \rightarrow (TC \boxtimes TC)_1 \rightarrow \dots \rightarrow (TC \boxtimes TC)_k \rightarrow \widetilde{CC}$  that realizes the  $\text{id}$  automorphism and that can form both a 1-component disorder model with  $A_0$  and a 1-component disorder model with  $A_2$ .

Assume that we have chosen some measurement sequence for  $\mathbb{1}$ . Eq. (A14) tells us that

$$\text{id} = \varphi_f[(rx)(gy)(bz)]^\alpha[(rz)(gy)(bx)]^\beta \varphi_i^{-1}. \quad (\text{B5})$$

We first simplify this by noting that for all  $\varphi_i, \varphi_f$  isomorphism contributions listed in Table A.1, none contain permutations affecting the  $z$  flavor label. This enforces that  $\alpha = \beta = 0$ . Then,  $\text{id} = \varphi_f \varphi_i^{-1}$  gives  $\varphi_f = \varphi_i$ . This means that the first condensation  $(TC \boxtimes TC)_1$  is the same as the final condensation  $(TC \boxtimes TC)_k$  in the measurement sequence.

We now consider the possible 1-component disorder models that can be made that involve our chosen measurement sequence. By Eq. (A14), there are only 6 possible effects that changing the disorder parameter from  $p = 0$  to  $p = 1$  (or equivalently,  $p = 1$  to  $p = 0$ ) can have on the enacted automorphism:

- (1)  $\alpha \mapsto \alpha + 1 \pmod{2}$ ;
- (2)  $\beta \mapsto \beta + 1 \pmod{2}$ ;
- (3)  $\alpha \mapsto \alpha + 1 \pmod{2}$  and  $\varphi_i \mapsto \varphi'_i$  by adding an additional condensation step in the first  $CC$  layer prior to  $(TC \boxtimes TC)_1$ ;
- (4)  $\alpha \mapsto \alpha + 1 \pmod{2}$  and  $\varphi_f \mapsto \varphi'_f$  by adding an additional condensation step in the first  $CC$  layer after  $(TC \boxtimes TC)_k$ ;
- (5)  $\beta \mapsto \beta + 1 \pmod{2}$  and  $\varphi_i \mapsto \varphi''_i$  by adding an additional condensation step in the second  $CC$  layer prior to  $(TC \boxtimes TC)_1$ ; and
- (6)  $\beta \mapsto \beta + 1 \pmod{2}$  and  $\varphi_f \mapsto \varphi''_f$  by adding an additional condensation step in the second  $CC$  layer after  $(TC \boxtimes TC)_k$ .

We can show that these 6 options realize only 4 different automorphisms. For each of (3)-(6) there is only one choice of condensation boson that we can introduce that is a mutual-semion with the condensates before and after it. Thus, since  $(TC \boxtimes TC)_1 = (TC \boxtimes TC)_k$  and  $\varphi_i = \varphi_f$ , we must have  $\varphi'_i = \varphi'_f$  and  $\varphi''_i = \varphi''_f$ . Let  $\varphi_{(3)}$  be the enacted automorphism when we follow option (3),

$$\varphi_{(3)} = \varphi_i[(rx)(gy)(bz)]\varphi_i'^{-1}, \quad (\text{B6})$$

where we use  $\varphi_i = \varphi_f$ . Similarly, let  $\varphi_{(4)}$  be the enacted automorphism for option (4),

$$\varphi_{(4)} = \varphi_i'[(rx)(gy)(bz)]\varphi_i^{-1}, \quad (\text{B7})$$

where we use  $\varphi'_i = \varphi'_f$ . Finally, by noting that all  $\varphi \in \mathcal{C}\{(\text{c}\sigma)(\text{c}\sigma)(\text{c}\sigma)\}$  satisfy  $\varphi = \varphi^{-1}$ , we have

$$\begin{aligned} \varphi_{(3)} &= \varphi_{(3)}^{-1} \\ &= (\varphi_i[(rx)(gy)(bz)]\varphi_i'^{-1})^{-1} \\ &= \varphi_i'[(rx)(gy)(bz)]\varphi_i^{-1} \\ &= \varphi_{(4)}. \end{aligned} \quad (\text{B8})$$

An equivalent argument shows that  $\varphi_{(5)} = \varphi_{(6)}$ . This means that a given measurement sequence for  $\mathbb{1}$  can only be in 1-component disorder models with 4 other FETs. However, there are 6 FETs that are connected to  $\mathbb{1}$  (corresponding to the 6 elements of  $\mathcal{C}\{(\text{c}\sigma)(\text{c}\sigma)(\text{c}\sigma)\}$ ). We therefore cannot construct a 2-component disorder model with  $\mathbb{1}$  and all possible  $A_0$  and  $A_2$ .

If we were to extend the disorder model definition to allow for a measurement sequence involving intermediary  $\widetilde{CC}$  stages, such as  $\widetilde{CC} \rightarrow \mathcal{A}_1 \rightarrow \dots \rightarrow \widetilde{CC} \rightarrow$

$\mathcal{B}_1 \rightarrow \dots \rightarrow \widetilde{CC}$ , then it becomes possible for any length- $m$  adjacency sequence to form an  $m$ -component disorder model.<sup>24</sup> This freedom, however, strays the model further from its interpretation as disordered DA color codes that are designed to implement logical gates on an encoded system.

This could be generalized further to allow condensation of any bosons of  $CC \boxtimes CC$ . For example, starting from  $\widetilde{CC}$  and condensing  $rx_1$  (with no boson in the second layer), then  $bx_1$ , then returning to  $\widetilde{CC}$  includes only reversible transitions (all logical operators update reversibly); this allows us to make changes to the measurement sequences in ways previously forbidden [i.e.,  $TC(rx) \rightarrow TC(bx)$  is not a reversible transition]. We may also consider models with anticorrelated disorder between two link types: measuring  $rx_1$  with probability  $p$  and  $bx_1$  with probability  $1 - p$ , for example. Even with condensed bosons in the second layer, this would not result in an irreversible phase because the regions of  $rx$ - and  $bx$ -measurements do not overlap. In the case of Eq. (B2), this would enable removing the  $gz_1$  condensation while retaining reversible transitions, and thus Eq. (B2) and Eq. (B3) can be connected.

### 3. Irreversible Phases

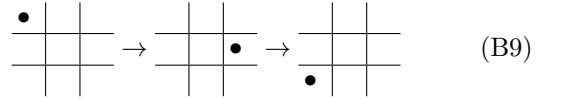
As discussed in Section IV, irreversible phases arise when the measurement sequences consecutively condense bosons that braid trivially. These generally result in logical information measured out due to the condensation of commuting anyons [26]. Moreover, there are also disruptions to the ISG of the code, such that we do not return to the  $\widetilde{CC}$  ISG after the period. For intralayer scenarios the plaquette operators are not reintroduced and links remain from the intermediary  $TC$  phases. For interlayer scenarios the two  $CC$  layers are not recoupled, resulting in logicals that may reside on only one layer, for example. We describe these behaviors in more detail here.

We first consider irreversible  $TC \boxtimes TC$  intralayer transitions, starting from the illustrative case of child theories of  $CC$ . Measuring a link corresponding to the hopping operator for anyon  $c\sigma$  has two effects on the ISG: (1) remove plaquettes of color  $c$  and flavor  $\sigma'$  for  $\sigma' \neq \sigma$ ; and (2) add plaquettes of color  $c'$  and flavor  $\sigma$  for  $c' \neq c$ .<sup>25</sup>

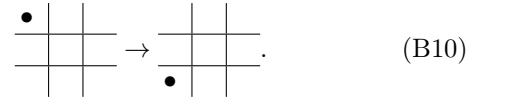
<sup>24</sup> Specifically, if  $\{A_0, A_1, \dots, A_m\}$  is an adjacency sequence (cf. Definition 2), we can construct the  $m$ -component disorder model by beginning with the measurement sequence for  $A_0$ . Once returned to  $\widetilde{CC}$ , we append the 1-component disorder model with automorphisms  $\text{id}$  for  $p_1 = 0$  and  $\tau_{10}$  for  $p_1 = 1$ . Repeating this for all  $\tau_{i(i-1)}$  up to  $i = m$  gives the required  $m$ -component disorder model. This is similar to the procedure in Eq. (26), but now the freedom to return to  $\widetilde{CC}$  allows us to concatenate multiple 1-component disorder models.

<sup>25</sup> Technically,  $c\sigma$ -links are added, not plaquette terms. However, the product of  $c\sigma$  links around a  $c' \neq c$  hexagon is equivalent to the  $c'\sigma$ -plaquette operator.

By tracking the presence of these plaquettes at each measurement stage, we can determine if the ISG is reproduced. For example, contrast the case of



with



In the following table we denote by  $\bullet$  the presence of each type of plaquette operator in the ISG at each stage of the measurement sequences. For the first example, we have:

	$rx$	$gx$	$bx$	$rz$	$gz$	$bz$
$TC(rx)$	$\bullet$	$\bullet$	$\bullet$		$\bullet$	$\bullet$
$TC(gz)$		$\bullet$	$\bullet$	$\bullet$	$\bullet$	$\bullet$
$TC(bx)$	$\bullet$	$\bullet$	$\bullet$	$\bullet$	$\bullet$	

(B11)

All plaquettes are recovered as expected and we realize the  $TC(bx)$  phase. In the second example, however, we have

	$rx$	$gx$	$bx$	$rz$	$gz$	$bz$
$TC(rx)$	$\bullet$	$\bullet$	$\bullet$		$\bullet$	$\bullet$
$TC(bx)$		$\bullet$	$\bullet$	$\bullet$		

(B12)

In this final state, there are individual  $rx$  and  $bx$ -type links, but no  $rz$ -type plaquettes. The effect of this is that a logical  $\bar{O}(bz)$ , for example, no longer has representatives that extend across all homologous cycles of the torus, since there are no  $rz$ -plaquettes in the ISG with which to multiply to deform one string into another.

Additional disruptions occur when we consider  $TC \boxtimes TC \rightarrow \widetilde{CC}$  interlayer irreversible transitions. In these, we have a situation where the measured  $Z_1 Z_2$  interlayer links will not always anticommute with some element of the ISG (with the precise scenario determined by the random disorder realization). These links are therefore not added to the ISG, and we produce a phase with interlinked  $CC$  layers that behaves differently to  $\widetilde{CC}$ . In particular, there exist X-logical operators that reside on just one layer, e.g.  $\bar{O}(bx_1)$ , or Z-logical operators that cannot freely switch between the two layers as they may in  $\widetilde{CC}$  (wherein  $rz_1 \sim rz_2$ , for example).

### Appendix C: Trajectories, Phase Transitions and Critical Behaviour

In this section, we introduce the idea of “trajectories” in parameter space as another interpretation of  $m$ -component disorder models. We then formalize the idea of competing automorphism phases (Section III) by linking the critical behavior of trajectories to the universality class of bond percolation, aided by numerical simulations.

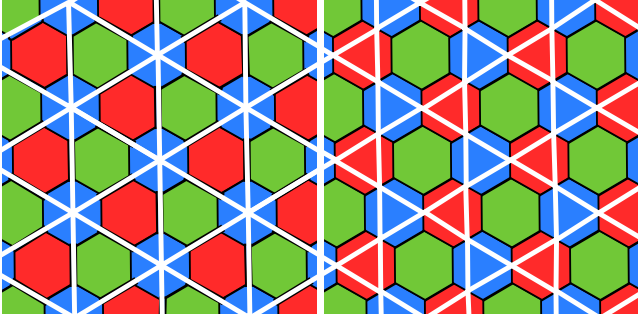


Figure C.1. Left. In a model with blue links disordered, we contract the remaining green and red links to a point to form a triangular superlattice (shown in white). Spanning domain walls are equivalent to percolating bonds on this superlattice. Right. In a model with blue and red links disordered, we contract the remaining green links to a point to form a kagome superlattice (shown in white).

In the main text, we treated an  $m$ -component disorder model as having  $m$  independent parameters. This is not required, however. Within an  $m$ -dimensional parameter space we can, for example, define a 1-parameter “trajectory”  $\mathbf{p}(p) \in [0, 1]^m$  that interpolates between the FETs at two different corners, with  $p \in [0, 1]$  such that  $\mathbf{p}(0)$  realizes FET  $A$  and  $\mathbf{p}(1)$  realizes FET  $B$ . For example, in the case of Eq. (30),  $\mathbf{p}(p) = (p, p)$  maps between the FETs with automorphism  $\text{id}$  at  $p = 0$  and  $(rgb)(xzy)$  at  $p = 1$ . The results for logically-connected FETs can also be readily modified to trajectories: we call a trajectory logically-protected if there exists a consistent nonzero-dimensional logical Hilbert subspace that remains unmeasured in the limit of  $t \rightarrow \infty$  periods at any point  $p \in [0, 1]$  of the trajectory. If two FETs are joined by a logically-protected trajectory, they must also be logically-connected. Conversely, an  $m$ -component disorder model containing an irreversible phase must support a trajectory that is not logically-protected.

Moreover, these trajectories allow us to smoothly interpolate the measurement sequence of one FET into that of another. As noted in Section IV B, we cannot distinguish two points  $p, \tilde{p} \in [0, 1]$  in a logically-protected trajectory solely using the time evolution of an observable from the protected algebra. This means that an “adiabatic transition” where a system evolves between two FETs using a time-dependent trajectory  $p(t) = t/T \in [0, 1]$  for  $t = 0, 1, \dots, T$  will not affect the periodic behavior of any logical operator that is protected. Observables that belong to not protected qubits, however, can distinguish these two phases. This allows us to detect phase transitions between different FETs and determine their critical behavior.

To determine the critical behavior, we first provide some intuition as to the universality class. In a 1-component disorder model, links of one color are selected randomly. We thus contract each of the other two colored links to a point to consider only the behavior of the

disordered links. In the honeycomb lattice, this contraction leaves behind the bonds of a triangular superlattice, cf. Fig. C.1. Each bond is chosen independently with the same probability, and a temporal domain wall containing a contiguous region extending around a noncontractible cycle is in direct correspondence to the existence of spanning clusters of these chosen bonds. Therefore, the critical behavior of a 1-component disorder model is expected to be in the same universality class as bond percolation on a triangular lattice with a critical parameter  $p_{c, \text{triangular}} = 0.347\dots$  and exponent  $\nu = 1.3$  [95, 96].

In a general  $m$ -component disorder model, more complicated behaviors emerge. Disordered links in different  $CC$  layers operate independently of each other, and therefore it is possible for multiple triangular-bond percolation problems to occur concurrently, potentially with different probability parameters dependent on the point in parameter space. If two different-colored links on the same layer are in consecutive disordered stages, however, then the universality class changes. Now, we contract only the one set of non-disordered links, and consider the spanning set of both disordered colors. These form the bonds of a kagome superlattice, cf. Fig. C.1. If both colors are chosen independently with the same probability, then the critical behavior now is expected to follow the universality class of bond percolation on a kagome lattice with critical parameter  $p_{c, \text{kagome}} = 0.524\dots$  and exponent  $\nu = 1.3$  [95, 96]. We note that these same two percolation behaviors can be applied to, and were indeed observed in, the disordered honeycomb Floquet code with missing measurements [35]. In our model, the increased parameter space enables combinations of both percolation problems to arise concurrently.

We now provide evidence for these claims by performing numerical simulations of disordered DA color codes. This analysis was done in Julia, using the `QuantumClifford.jl` package [97] for efficient computation with the stabilizer formalism [2, 12, 84, 98]. The system is on a honeycomb lattice characterized by linear system size  $L$ , such that there are  $L$  plaquettes in each of the horizontal and vertical directions,<sup>26</sup> and joined by periodic boundary conditions on all sides. Unless specified otherwise, simulations were repeated  $N = 508$  times using  $L = 18$ .

We use two metrics: firstly, the Fourier components of the average-squared-expectation of an observable  $O$  for a given initial state  $|\psi\rangle$ :

$$g_{O, |\psi\rangle}(\lambda) = \lim_{T \rightarrow \infty} \frac{2}{T} \sum_{t=0}^{T-1} e^{2i\pi t/\lambda} G_{O, |\psi\rangle}(t) \quad (\text{C1})$$

where

$$G_{O, |\psi\rangle}(t) = \overline{\langle \psi(t) | O | \psi(t) \rangle^2} \quad (\text{C2})$$

<sup>26</sup> Equivalently,  $2L$  lattice sites in the horizontal direction and  $L$  lattice sites vertically.

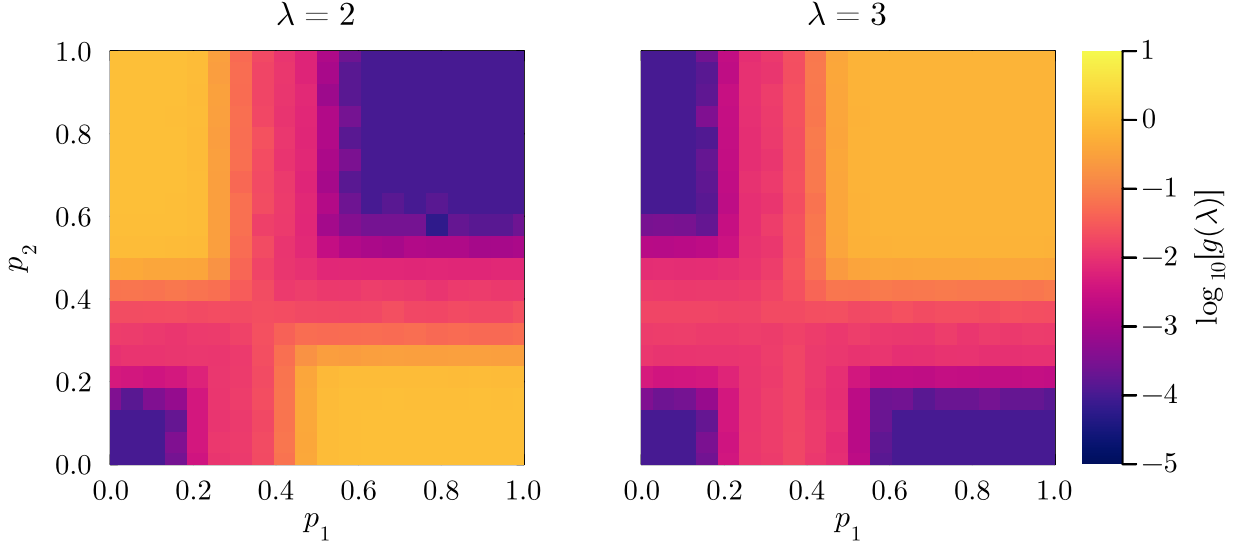


Figure C.2.  $\pi$  and  $2\pi/3$  ( $\lambda = 2$  and  $\lambda = 3$ ) Fourier components of the average-squared-expectation of the  $\bar{X}_3$  logical operator computed from an initial logical state of  $|++++\rangle$  and evolving under Eq. (29) for  $t \leq 96$  time steps. This initial state and observable were chosen to demonstrate the different FETs at the corners of the parameter space. We see nonzero period-2 oscillations in the  $(p_1, p_2) = (0, 1)$  and  $(1, 0)$  corners, and nonzero period-3 oscillations in the  $(1, 1)$  corner, consistent with the predicted automorphisms, cf. Eqs. (30), (C4), (C5), and (C6).

and  $\psi(t)$  is the evolution of the initial state after an integer  $t \geq 0$  periods of a given measurement sequence. We can use  $g(\lambda)$  to distinguish between the subcritical and supercritical phases of a trajectory by choosing a state and observable that evolve differently under the automorphisms at the two endpoints. For example, a 3-cycle automorphism at  $\mathbf{p}(0)$  and a 2-cycle automorphism at  $\mathbf{p}(1)$  can result in a nonvanishing  $g(3)$  when  $p = 0$  and a nonvanishing  $g(2)$  when  $p = 1$ . In practice, we need to truncate the limit at some finite  $T'$  that must be a multiple of the periods under study; this ensures that the Fourier decomposition equation is valid. We chose  $T' = 96$  for our simulations: a multiple of 2, 3, 4, and 6.

Secondly, we consider the purification dynamics of the system. We track the evolution starting from a maximally-mixed logical state  $\rho$  by measuring its (average) von Neumann entropy  $S = \rho \log \rho$  over time [99]. At  $t = 0$ , we start from the maximum 4. Over multiple periods of the measurement sequence, entropy reduces if logical qubits are measured. A logically-protected trajectory must retain  $S(t) > 0$  in the limit  $t \rightarrow \infty$  at all points  $p$ . To model this, we assume the form

$$S(t) = S_\infty + (S_0 - S_\infty)e^{-\Gamma t} \quad (\text{C3})$$

and consider the decay rate  $\Gamma$  or associated timescale  $\tau = 1/\Gamma$ . We again truncate using  $t \leq 96$  to approximate  $S_\infty$  and  $\tau$  in numerical simulations.

We consider now an example of a 2-component disorder model. Specifically, take the measurement sequence given by Eq. (29) with automorphisms in Eq. (30). All corners of the 2-dimensional parameter space are FETs, and the associated automorphisms are even-parity on the  $S_3 \times S_3$  subgroup. We choose  $|\psi\rangle$  such that it is an eigen-

state of logical operators that evolve differently in the corners of the phase diagram. This is easily observed using the stabilizer picture [86]; take  $\bar{X}_3 = \bar{O}[\mathbf{bx}]_h$ , for example. It does not change when evolving under the identity. Under  $(rx)(gy)(bz)$  we see

$$\bar{O}[\mathbf{bx}]_h \mapsto \bar{O}[\mathbf{rz}]_h \mapsto \bar{O}[\mathbf{bx}]_h \mapsto \dots \quad (\text{C4})$$

while under  $(rz)(gx)(by)$  it evolves as

$$\bar{O}[\mathbf{bx}]_h \mapsto \bar{O}[\mathbf{gy}]_h \mapsto \bar{O}[\mathbf{bx}]_h \mapsto \dots \quad (\text{C5})$$

Finally, under  $(rgb)(xzy)$  we get

$$\bar{O}[\mathbf{bx}]_h \mapsto \bar{O}[\mathbf{rz}]_h \mapsto \bar{O}[\mathbf{gy}]_h \mapsto \bar{O}[\mathbf{bx}]_h \mapsto \dots \quad (\text{C6})$$

Notably, it returns to an eigenstate of  $\bar{X}_3$  only after 2 Floquet periods in  $(rx)(gy)(bz)$  and  $(rz)(gx)(by)$ , and after 3 periods in  $(rgb)(xzy)$ . At other times the operator maps to  $\bar{Y}$  or  $\bar{Z}$ , and the expectation of  $\bar{X}_3$  is 0. Starting in a +1-eigenstate of  $\bar{X}_1$ ,  $\bar{X}_2$ ,  $\bar{X}_3$ , and  $\bar{X}_4$  (denoted  $|++++\rangle$ ), the squared expectation of  $\bar{X}_3$  should show period-doubling oscillations between 1 and 0 at  $\mathbf{p} = (0, 1)$  and  $(1, 0)$ , and period-tripling behavior at  $\mathbf{p} = (1, 1)$ . The Fourier components of  $G_{\bar{X}_3, |++++\rangle}$  are plotted in Fig. C.2, with nonvanishing values of  $g(2)$  and  $g(3)$  appearing only in these predicted corners.

These automorphisms in Eq. (30) satisfy the conditions in Section IV B and therefore it is possible for there to exist a logically-protected trajectory through the parameter space. We first plot the purification dynamics in Fig. C.3, for illustrative values of  $\mathbf{p}$ . As expected from Section III, two logical qubits are measured out near the critical point, which we find to be around  $p \sim 0.37$ . Taking a parameter sweep of all  $p_1, p_2 \in [0, 1]$ , we get

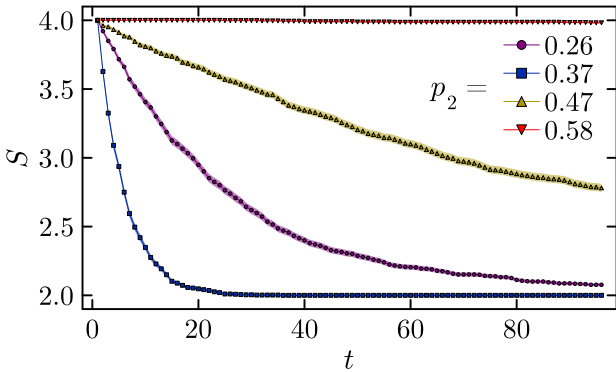


Figure C.3. Average von Neumann entropy  $S = \rho \log \rho$  of a maximally-mixed logical state with  $S_0 = 4$  and evolving under Eq. (29) at various values of  $p_2$  with  $p_1 = 0$  (thus reducing to a 1-component disorder model). Ribbon shows the standard error of the mean based on  $N = 508$  repetitions. Near the critical value of  $p_c = 0.347\dots$ , the entropy approaches the long-term value of  $S_\infty = 2$ . Away from there, the entropy remains at  $S = 4$ .

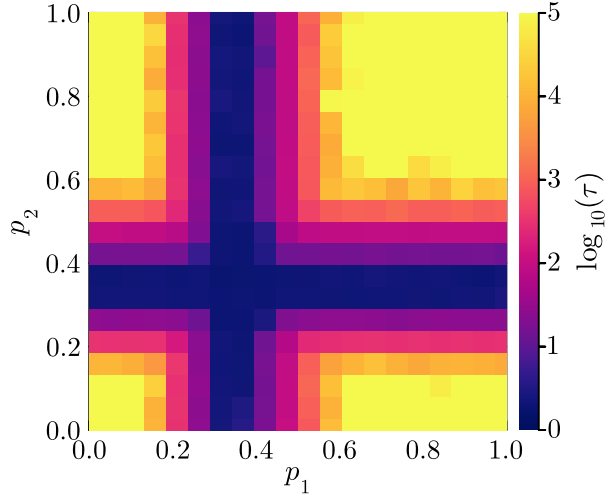


Figure C.4. Average purification timescale  $\tau = 1/\Gamma$  from Eq. (C3) for a maximally-mixed logical state with  $S_0 = 4, S_\infty = 2$  evolving under Eq. (29) at various values of  $p_1, p_2$ , up to  $t \leq 96$ . Exactly 2 logical qubits are measured out when tuned near the critical lines at  $p_c \sim 0.35$  (dark blue regions).

Fig. C.4 that shows the average purification decay rate  $\tau = 1/\Gamma$ . Near the critical lines  $p \sim 0.35$ , we get a finite decay rate, with  $\tau \rightarrow \infty$  elsewhere. To determine this critical value more precisely, we take the trajectory  $\mathbf{p}(p) = (0, p)$ . Figure C.5 shows the average purification dynamics at different values of linear system size  $L$ , and presents a scaling-collapse of the form  $(p - p_c)L^{1/\nu}$  that shows scale-invariant behaviour [35]. Using finite size scaling methods [95], we estimate critical values of  $p_c = 0.346(4)$  and  $\nu = 1.31(9)$ , consistent with the theoretical values for bond percolation on a triangular lattice [96]. The trajectory  $\mathbf{p}(p) = (p, p)$  that traverses along

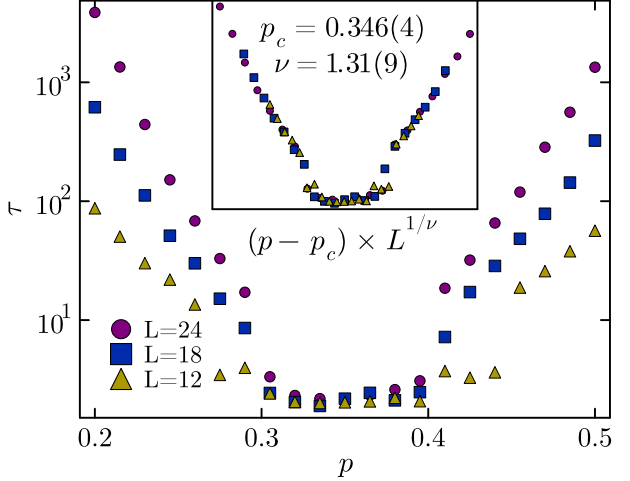


Figure C.5. Average purification timescale  $\tau$  for a maximally-mixed logical state evolving under Eq. (29) with the trajectory  $\mathbf{p}(p) = (0, p)$  near the critical point. We run the simulation at various values of linear system size,  $L$ . Inset shows the finite-size scaling collapse under the estimated parameters of  $p_c = 0.346(4)$  and  $\nu = 1.31(9)$  using the functional form  $(p - p_c)L^{1/\nu}$ . These are consistent with the theoretical  $p_c = 0.347\dots$  and  $\nu = 1.3$  for bond percolation on the triangular lattice.

the diagonal of Fig. C.5 will also exhibit the same critical values.

- 
- [1] A. M. Steane, Error Correcting Codes in Quantum Theory, *Physical Review Letters* **77**, 793 (1996).
- [2] D. E. Gottesman, *Stabilizer Codes and Quantum Error Correction*, Ph.D. thesis, California Institute of Technology (1997).
- [3] A. Y. Kitaev, Quantum computations: Algorithms and error correction, *Russian Mathematical Surveys* **52**, 1191 (1997).
- [4] A. Yu. Kitaev, Quantum Error Correction with Imperfect Gates, in *Quantum Communication, Computing, and Measurement*, edited by O. Hirota, A. S. Holevo, and C. M. Caves (Springer US, Boston, MA, 1997) pp. 181–188.
- [5] E. Knill and R. Laflamme, Theory of quantum error-correcting codes, *Physical Review A* **55**, 900 (1997).
- [6] J. Preskill, Fault-Tolerant Quantum Computation, in *Introduction to Quantum Computation and Information* (WORLD SCIENTIFIC, 1998) pp. 213–269.
- [7] P. W. Shor, Fault-tolerant quantum computation (1997), [arXiv:quant-ph/9605011](https://arxiv.org/abs/quant-ph/9605011).
- [8] E. Knill, R. Laflamme, and L. Viola, Theory of Quantum Error Correction for General Noise, *Physical Review Letters*

- ters **84**, 2525 (2000).
- [9] T. Schuster, C. Yin, X. Gao, and N. Y. Yao, A polynomial-time classical algorithm for noisy quantum circuits (2024), [arXiv:2407.12768](#).
- [10] X. G. Wen, Vacuum degeneracy of chiral spin states in compactified space, *Physical Review B* **40**, 7387 (1989).
- [11] E. Witten, Quantum field theory and the Jones polynomial, *Communications in Mathematical Physics* **121**, 351 (1989).
- [12] D. Poulin, Stabilizer Formalism for Operator Quantum Error Correction, *Physical Review Letters* **95**, 230504 (2005), [arXiv:quant-ph/0508131](#).
- [13] X. Fu and D. Gottesman, Error Correction in Dynamical Codes (2024), [arXiv:2403.04163](#) [quant-ph].
- [14] M. Davydova, N. Tantivasadakarn, and S. Balasubramanian, Floquet Codes without Parent Subsystem Codes, *PRX Quantum* **4**, 020341 (2023).
- [15] G.-Y. Zhu and S. Trebst, Qubit fractionalization and emergent Majorana liquid in the honeycomb Floquet code induced by coherent errors and weak measurements (2023), [arXiv:2311.08450](#) [cond-mat, physics:quant-ph].
- [16] G.-Y. Zhu, N. Tantivasadakarn, A. Vishwanath, S. Trebst, and R. Verresen, Nishimori's Cat: Stable Long-Range Entanglement from Finite-Depth Unitaries and Weak Measurements, *Physical Review Letters* **131**, 200201 (2023).
- [17] M. B. Hastings and J. Haah, Dynamically Generated Logical Qubits, *Quantum* **5**, 564 (2021).
- [18] C. Vuillot, Planar Floquet Codes (2021), [arXiv:2110.05348](#) [quant-ph].
- [19] J. Haah and M. B. Hastings, Boundaries for the Honeycomb Code, *Quantum* **6**, 693 (2022), [arXiv:2110.09545](#) [quant-ph].
- [20] T. D. Ellison, J. Sullivan, and A. Dua, Floquet codes with a twist (2023), [arXiv:2306.08027](#) [quant-ph].
- [21] S. B. Bravyi and A. Y. Kitaev, Quantum codes on a lattice with boundary, [arXiv:quant-ph/9811052](#) (1998), [arXiv:quant-ph/9811052](#).
- [22] E. Dennis, A. Kitaev, A. Landahl, and J. Preskill, Topological quantum memory, *Journal of Mathematical Physics* **43**, 4452 (2002), [arXiv:quant-ph/0110143](#).
- [23] A. Y. Kitaev, Fault-tolerant quantum computation by anyons, *Annals of Physics* **303**, 2 (2003), [arXiv:quant-ph/9707021](#).
- [24] A. Kitaev, Anyons in an exactly solved model and beyond, *Annals of Physics* **321**, 2 (2006).
- [25] M. S. Kesselring, F. Pastawski, J. Eisert, and B. J. Brown, The boundaries and twist defects of the color code and their applications to topological quantum computation, *Quantum* **2**, 101 (2018).
- [26] M. S. Kesselring, J. C. Magdalena De La Fuente, F. Thomsen, J. Eisert, S. D. Bartlett, and B. J. Brown, Anyon Condensation and the Color Code, *PRX Quantum* **5**, 010342 (2024), [arXiv:2212.00042](#) [cond-mat, physics:quant-ph].
- [27] H. Bombin, Topological Order with a Twist: Ising Anyons from an Abelian Model, *Physical Review Letters* **105**, 030403 (2010), [arXiv:1004.1838](#).
- [28] B. J. Brown, S. D. Bartlett, A. C. Doherty, and S. D. Barrett, Topological Entanglement Entropy with a Twist, *Physical Review Letters* **111**, 220402 (2013), [arXiv:1303.4455](#).
- [29] D. Aasen, Z. Wang, and M. B. Hastings, Adiabatic paths of Hamiltonians, symmetries of topological order, and automorphism codes, *Physical Review B* **106**, 085122 (2022).
- [30] A. C. Potter and T. Morimoto, Dynamically enriched topological orders in driven two-dimensional systems, *Physical Review B* **95**, 155126 (2017).
- [31] H. C. Po, L. Fidkowski, A. Vishwanath, and A. C. Potter, Radical chiral Floquet phases in a periodically driven Kitaev model and beyond, *Physical Review B* **96**, 245116 (2017).
- [32] M. Davydova, N. Tantivasadakarn, S. Balasubramanian, and D. Aasen, Quantum computation from dynamic automorphism codes, *Quantum* **8**, 1448 (2024).
- [33] D. Aasen, J. Haah, P. Bonderson, Z. Wang, and M. Hastings, Fault-Tolerant Hastings-Haah Codes in the Presence of Dead Qubits (2023), [arXiv:2307.03715](#) [quant-ph].
- [34] C. McLauchlan, G. P. Gehér, and A. E. Moylett, Accommodating Fabrication Defects on Floquet Codes with Minimal Hardware Requirements (2024), [arXiv:2405.15854](#) [quant-ph].
- [35] D. Vu, A. Lavasani, J. Y. Lee, and M. P. A. Fisher, Stable Measurement-Induced Floquet Enriched Topological Order, *Physical Review Letters* **132**, 070401 (2024), [arXiv:2303.01533](#) [cond-mat, physics:quant-ph].
- [36] A. Sriram, T. Rakovszky, V. Khemani, and M. Ippoliti, Topology, criticality, and dynamically generated qubits in a stochastic measurement-only Kitaev model, *Physical Review B* **108**, 094304 (2023), [arXiv:2207.07096](#) [cond-mat, physics:quant-ph].
- [37] Y. Li, X. Chen, and M. P. A. Fisher, Quantum Zeno effect and the many-body entanglement transition, *Physical Review B* **98**, 205136 (2018).
- [38] Y. Li, X. Chen, and M. P. A. Fisher, Measurement-driven entanglement transition in hybrid quantum circuits, *Physical Review B* **100**, 134306 (2019).
- [39] S. Choi, Y. Bao, X.-L. Qi, and E. Altman, Quantum Error Correction in Scrambling Dynamics and Measurement-Induced Phase Transition, *Physical Review Letters* **125**, 030505 (2020).
- [40] C.-M. Jian, Y.-Z. You, R. Vasseur, and A. W. W. Ludwig, Measurement-induced criticality in random quantum circuits, *Physical Review B* **101**, 104302 (2020).
- [41] M. Ippoliti, M. J. Gullans, S. Gopalakrishnan, D. A. Huse, and V. Khemani, Entanglement Phase Transitions in Measurement-Only Dynamics, *Physical Review X* **11**, 011030 (2021).
- [42] M. P. Fisher, V. Khemani, A. Nahum, and S. Vijay, Random Quantum Circuits, *Annual Review of Condensed Matter Physics* **14**, 335 (2023).
- [43] B. Skinner, J. Ruhman, and A. Nahum, Measurement-Induced Phase Transitions in the Dynamics of Entanglement, *Physical Review X* **9**, 031009 (2019).
- [44] Y. Bao, S. Choi, and E. Altman, Theory of the phase transition in random unitary circuits with measurements, *Physical Review B* **101**, 104301 (2020).
- [45] M. Ippoliti and V. Khemani, Postselection-Free Entanglement Dynamics via Spacetime Duality, *Physical Review Letters* **126**, 060501 (2021).
- [46] Y. Li, Y. Zou, P. Glorioso, E. Altman, and M. P. A. Fisher, Cross Entropy Benchmark for Measurement-Induced Phase Transitions, *Physical Review Letters* **130**, 220404 (2023).
- [47] Y. Li and M. P. A. Fisher, Statistical mechanics of quantum error correcting codes, *Physical Review B* **103**, 104306 (2021).

- [48] M. J. Gullans and D. A. Huse, Dynamical Purification Phase Transition Induced by Quantum Measurements, *Physical Review X* **10**, 041020 (2020).
- [49] A. Nahum and B. Skinner, Entanglement and dynamics of diffusion-annihilation processes with Majorana defects, *Physical Review Research* **2**, 023288 (2020).
- [50] A. Nahum, S. Roy, B. Skinner, and J. Ruhman, Measurement and Entanglement Phase Transitions in All-To-All Quantum Circuits, on Quantum Trees, and in Landau-Ginsburg Theory, *PRX Quantum* **2**, 010352 (2021).
- [51] A. Zabalo, M. J. Gullans, J. H. Wilson, S. Gopalakrishnan, D. A. Huse, and J. H. Pixley, Critical properties of the measurement-induced transition in random quantum circuits, *Physical Review B* **101**, 060301 (2020).
- [52] G. M. Sommers, D. A. Huse, and M. J. Gullans, Dynamically generated concatenated codes and their phase diagrams (2024), arXiv:2409.13801 [cond-mat, physics:quant-ph].
- [53] J. Behrends, F. Venn, and B. Béri, Surface codes, quantum circuits, and entanglement phases, *Physical Review Research* **6**, 013137 (2024).
- [54] A. Lavasani, Y. Alavirad, and M. Barkeshli, Measurement-induced topological entanglement transitions in symmetric random quantum circuits, *Nature Physics* **17**, 342 (2021), arXiv:2004.07243 [cond-mat, physics:quant-ph].
- [55] H. Bombin and M. A. Martin-Delgado, Topological Quantum Distillation, *Physical Review Letters* **97**, 180501 (2006).
- [56] H. Bombín, Gauge color codes: Optimal transversal gates and gauge fixing in topological stabilizer codes, *New Journal of Physics* **17**, 083002 (2015).
- [57] B. Yoshida, Topological color code and symmetry-protected topological phases, *Physical Review B* **91**, 245131 (2015).
- [58] H. Bombín, G. Duclos-Cianci, and D. Poulin, Universal topological phase of two-dimensional stabilizer codes, *New Journal of Physics* **14**, 073048 (2012).
- [59] A. Kubica, B. Yoshida, and F. Pastawski, Unfolding the color code, *New Journal of Physics* **17**, 083026 (2015).
- [60] J. Haah, Classification of translation invariant topological Pauli stabilizer codes for prime dimensional qudits on two-dimensional lattices, *Journal of Mathematical Physics* **62**, 012201 (2021).
- [61] S. H. Simon, *Topological Quantum* (Oxford University Press, Oxford, United Kingdom, 2023).
- [62] N. D. Mermin, Simple unified form for the major no-hidden-variables theorems, *Physical Review Letters* **65**, 3373 (1990).
- [63] A. Peres, Two simple proofs of the Kochen-Specker theorem, *Journal of Physics A: Mathematical and General* **24**, L175 (1991).
- [64] M. Barkeshli, P. Bonderson, M. Cheng, and Z. Wang, Symmetry fractionalization, defects, and gauging of topological phases, *Physical Review B* **100**, 115147 (2019).
- [65] H. Bombin, Topological subsystem codes, *Physical Review A* **81**, 032301 (2010).
- [66] F. A. Bais and J. K. Slingerland, Condensate-induced transitions between topologically ordered phases, *Physical Review B* **79**, 045316 (2009).
- [67] Y. Hu, Z. Huang, L.-Y. Hung, and Y. Wan, Anyon condensation: Coherent states, symmetry enriched topological phases, Goldstone theorem, and dynamical rearrangement of symmetry, *Journal of High Energy Physics* **2022**, 26 (2022).
- [68] I. S. Eliëns, J. C. Romers, and F. A. Bais, Diagrammatics for Bose condensation in anyon theories, *Physical Review B* **90**, 195130 (2014).
- [69] T. D. Ellison, Y.-A. Chen, A. Dua, W. Shirley, N. Tantivasadakarn, and D. J. Williamson, Pauli topological subsystem codes from Abelian anyon theories, *Quantum* **7**, 1137 (2023).
- [70] L. Kong, Anyon condensation and tensor categories, *Nuclear Physics B* **886**, 436 (2014).
- [71] F. A. Bais, J. K. Slingerland, and S. M. Haaker, Theory of Topological Edges and Domain Walls, *Physical Review Letters* **102**, 220403 (2009).
- [72] D. Aasen, J. Haah, Z. Li, and R. S. K. Mong, Measurement Quantum Cellular Automata and Anomalies in Floquet Codes (2023), arXiv:2304.01277 [cond-mat, physics:math-ph, physics:quant-ph].
- [73] F. Burnell, Anyon Condensation and Its Applications, *Annual Review of Condensed Matter Physics* **9**, 307 (2018).
- [74] A. Bauer, The x+y Floquet code: A simple example for topological quantum computation in the path integral approach (2024), arXiv:2408.07265 [quant-ph].
- [75] J. C. M. de la Fuente, J. Old, A. Townsend-Teague, M. Rispler, J. Eisert, and M. Müller, The XYZ ruby code: Making a case for a three-colored graphical calculus for quantum error correction in spacetime (2024), arXiv:2407.08566 [cond-mat, physics:math-ph, physics:quant-ph].
- [76] A. Dua, N. Tantivasadakarn, J. Sullivan, and T. D. Ellison, Engineering 3D Floquet Codes by Rewinding, *PRX Quantum* **5**, 020305 (2024).
- [77] O. Higgott and N. P. Breuckmann, Constructions and performance of hyperbolic and semi-hyperbolic Floquet codes (2023), arXiv:2308.03750 [quant-ph].
- [78] J. Sullivan, R. Wen, and A. C. Potter, Floquet codes and phases in twist-defect networks (2023), arXiv:2303.17664 [cond-mat, physics:quant-ph].
- [79] A. Bauer, Topological error correcting processes from fixed-point path integrals, *Quantum* **8**, 1288 (2024), arXiv:2303.16405.
- [80] A. Bauer, Low-overhead non-Clifford topological fault-tolerant circuits for all non-chiral abelian topological phases (2024), arXiv:2403.12119 [cond-mat, physics:quant-ph].
- [81] A. Townsend-Teague, J. Magdalena De La Fuente, and M. S. Kesselring, Floquetifying the Colour Code, *Electronic Proceedings in Theoretical Computer Science* **384**, 265 (2023), arXiv:2307.11136 [math-ph, physics:quant-ph].
- [82] H. Bombin, D. Litinski, N. Nickerson, F. Pastawski, and S. Roberts, Unifying flavors of fault tolerance with the ZX calculus, *Quantum* **8**, 1379 (2024).
- [83] V. Motamarri, C. McLauchlan, and B. Béri, SymTFT out of equilibrium: From time crystals to braided drives and Floquet codes (2024), arXiv:2312.17176 [cond-mat, physics:hep-th, physics:quant-ph].
- [84] D. Gottesman, The Heisenberg Representation of Quantum Computers, in *Proceedings of the XXII International Colloquium on Group Theoretical Methods in Physics*, edited by S. P. Corney, R. Delbourgo, and P. D. Jarvis (International Press, Cambridge, MA, 1998) pp. 32–43, arXiv:quant-ph/9807006.
- [85] C. T. Chubb and S. T. Flammia, Statistical mechanical

- models for quantum codes with correlated noise, *Annales de l'Institut Henri Poincaré D, Combinatorics, Physics and their Interactions* **8**, 269 (2021).
- [86] M. A. Nielsen and I. L. Chuang, *Quantum Computation and Quantum Information*, 10th ed. (Cambridge University Press, Cambridge ; New York, 2010).
- [87] F. Loulidi, I. Nechita, and C. Pellegrini, *A physical noise model for quantum measurements* (2024), arXiv:2305.19766 [quant-ph].
- [88] M. Grassl, Th. Beth, and T. Pellizzari, Codes for the quantum erasure channel, *Physical Review A* **56**, 33 (1997).
- [89] S. Gu, A. Retzker, and A. Kubica, *Fault-tolerant quantum architectures based on erasure qubits* (2023), arXiv:2312.14060 [quant-ph].
- [90] F. Venn, J. Behrends, and B. Béri, Coherent-Error Threshold for Surface Codes from Majorana Delocalization, *Physical Review Letters* **131**, 060603 (2023).
- [91] T. Botzung, M. Buchhold, S. Diehl, and M. Müller, Robustness and measurement-induced percolation of the surface code (2023), arXiv:2311.14338 [cond-mat, physics:quant-ph].
- [92] Y. Zhao and Y. Wan, Nonabelian Anyon Condensation in 2+1d topological orders: A String-Net Model Realization (2024), arXiv:2409.05852 [cond-mat].
- [93] Z. Zhang, D. Aasen, and S. Vijay, X-cube Floquet code: A dynamical quantum error correcting code with a subextensive number of logical qubits, *Physical Review B* **108**, 205116 (2023).
- [94] J. F. Humphreys, *A Course in Group Theory*, Oxford Science Publications (Oxford University Press, Oxford; New York, 1996).
- [95] D. Stauffer and A. Aharony, *Introduction to Percolation Theory*, rev. 2. ed., transferred to digital print ed. (Taylor & Francis, London, 2003).
- [96] M. F. Sykes and J. W. Essam, Exact Critical Percolation Probabilities for Site and Bond Problems in Two Dimensions, *Journal of Mathematical Physics* **5**, 1117 (1964).
- [97] S. Krastanov, Quantumclifford.jl, <https://github.com/QuantumSavory/QuantumClifford.jl> (2024).
- [98] S. Aaronson and D. Gottesman, Improved simulation of stabilizer circuits, *Physical Review A* **70**, 052328 (2004).
- [99] D. Fattal, T. S. Cubitt, Y. Yamamoto, S. Bravyi, and I. L. Chuang, Entanglement in the stabilizer formalism (2004), arXiv:quant-ph/0406168.